Greenhouse Gas Production and Transport Within Tile Drained Agriculture Systems

By

Oliver Blume

A thesis submitted to the Faculty of Graduate and Postdoctoral Affairs in partial fulfillment of the requirements for the degree of

Master of Science

In

Earth Sciences

Carleton University
Ottawa, Ontario

Abstract

Agriculture systems are becoming a growing concern regarding greenhouse gas (GHG) emissions; specifically, methane (CH_4), carbon dioxide (CO_2) and nitrous oxide (N_2O). This study focused on GHG transport within two controlled tile drained agriculture sites in Eastern Ontario. Subsurface and surface greenhouse gas fluxes were monitored throughout a transect at each site with sampling locations in the farm field and the shoulder and slope of the riparian zone in the fall of 2017 and the 2018 agronomic season. All sampling locations showed similar levels of CO_2 and N_2O emissions; however, CH_4 is observed as effluxes in oxidizing soils and influxes in reducing soils. GHG transport increases as soil depth decreases with maximum fluxes occurring at the soil/atmosphere interface. GHG transport is elevated in soil horizons that display larger concentration gradients and lower water saturation levels. Surface emissions are primarily influenced by GHGs produced and transported in shallow soil horizons.

Acknowledgments

I would like to show gratitude and appreciation for all people whole helped make this thesis possible. First, my thesis supervisor Dr. Richard Amos for his ongoing support throughout the research and writing process. Dr. David Lapen for his insight on field practices and encouragement to find my niche within the larger Agriculture Greenhouse Gap Program (AGGP) project. Dr. Ian Clark for taking the time to discuss my findings and help with data interpretations. Emilia Craiovan and Mark Sunohara for their ongoing support with field practices. They are the backbone behind all AGGP field operations and none of this would have been possible without their support. Dr. David Blowes, Dr. Carol Ptacek, Dr. Ulrich Mayer and Dr. David Rudolph for their insight on this data set. The AGGP students; David Geuder, Iwona Widurska, Eric Guitard, Vincent Nogueira and Anne-Martine Doucet for their collaborative efforts to ensure all field and research objectives were accomplished. Krista Elena, Sara Fellin and Joy Hu for their prompt and quality geochemical analyses of aqueous samples. The Agriculture and Agri-Food Canada (AAFC) lab team accommodating our dense sample set and conducting the appropriate analyses. The landowners for allowing us to use their fields for research purposes.

Last but not least, I am extremely grateful for all the support from my friends and family, especially my parents. This thesis would not have been possible without your continuous encouragement, thank you!

Preface

This thesis is comprised of two research chapters which were written to be easily manipulated into two publishable manuscripts after thesis submission. Chapter 2 addresses the data set as a whole, relating different geochemical data to greenhouse gas production, consumption and transport. Chapter 3 relates ^{14}C to the CO_2 data set to support transport interpretations made in Chapter 2. There may be some content overlap between the two chapters; however, they each possess a unique scope. The thesis will begin with a brief introduction (Chapter 1) summarizing the larger Agriculture Greenhouse Gas Program (AGGP) project and how this study ties into the other research initiatives. Chapter 4 will recap key findings and state recommendations for future studies.

This study includes a dense data set that was collected by numerous research participants working in association with the AGGP. Dr. David Lapen, Emilia Craiovan and Mark Sunohara facilitated the data collection with the help of countless co-op and honours students. Anne-Martine Doucet; a 2018-2019 honours student at the University of Ottawa, and Emilia Craiovan collected most of the surface GHG samples and calculated surface fluxes. Eric Guitard; a 2018-2019 honours student at the University of Ottawa, conducted all sample preparation and collection for $^{14}CO_2$ analyses and the IsoJar experiment. Piezometers were installed by David Gueder; a master's student (2017-present) from the University of Waterloo.

Table of Contents

List of Tables

List of Figures

1.0 Introduction

Greenhouse gas (GHG) emissions are a topic of concern as they are related to environmental issues such as water contamination (Gilliam et al., 1979; Nangia et al., 2013; Sunohara et al., 2014, 2015) and climate change (Cole et al., 1997; Paustian et al., 2016). The agriculture industry is one of the major contributors to global gas emissions (Duxbury, 1994; Paustian et al., 2016; Smith, et al., 2014). The Intergovernmental Panel on Climate Change (IPCC) monitors GHG inventories and shows that the agriculture industry has only decreased total emissions by 1% from 2005 to 2016 (ECCC, 2018). Every other IPCC sector has shown a much greater decrease in GHG emissions except for energy (transport). Even though there has been an ongoing effort to diminish negative environmental impacts related to agriculture activity, it is evident we need to develop a better understanding of these systems to enhance our ability to reduce GHG emissions. Changes in agriculture practices can have variable influences on GHG emissions due to their ability to alter soil conditions and structure (Ball, 2013; Gregorich et al., 2005). In order to develop mitigation strategies, we must conduct thorough investigations on site specific subsurface GHG behavior and relate them to surface emissions.

The agriculture greenhouse gas program (AGGP) is a five-year government initiative that began in 2017 to study the environmental implications of standard agricultural practices across Canada. There are many AGGP studies, each consisting of different research teams with different objectives. Our AGGP project; Valuing Diversity in Agroecosystems, is focused on investigating the significance of riparian zone (area between land and rivers or streams) vegetation on buffering agriculture contaminants and

their effect on GHG fluxes. This study is a collaborative effort between Agriculture and Agri-Food Canada (AAFC), Carleton University, the University of Waterloo, University of Ottawa, and the University of British Columbia, to create a multidisciplinary research team with the hopes of developing new best management practices (BMPs).

This study is primarily conducted on the Watershed Evaluation of Beneficial Management Practices (WEBs) field area; a succession of active agriculture sites in Eastern Ontario previously used by AAFC for other research projects. AAFC is a vital component of our AGGP project as they have experience working with these site-specific agriculture systems.

Our AGGP project is concentrating on four agriculture fields within the larger WEBs study area and an experimental field site at Winchester. Each WEBs field contains a different riparian ecosystem. The four fields are spatially divided into two pairs. The two fields within each pair lie parallel to each other (2 km apart) and drain into the same drainage ditch. One drainage ditch will continue to exhibit natural riparian vegetation coverage where the other is dredged. The Winchester sites will focus on the effects of bioreactors on attenuating agriculture contaminants and reducing GHG outputs.

The AGGP project involves three phases;

1. Baseline physical, biologic and geochemical characterization of WEBs prior to dredging. Analysis of the relationship between vegetation cover, soil conditions and

biologic/geochemical interactions on GHG transport and emissions. Use of this baseline data to calibrate a reactive-transport model of WEBs

2. Monitoring physical, biologic and geochemical changes that arise between the dredged and non-dredged sites.

3. Implementation of mitigation strategies determined by the analysis of phase two data and the Winchester experiments. Use of phase two data to advance model development and relate land use change to GHG fluxes.

The scope of my project is the baseline characterization of a non-dredged and dredged site prior to dredging. Subsurface and subsurface GHG measurements, soil and aqueous geochemistry, $^{14}CO_2$, and site-specific physical parameters will help show the spatial and temporal effects of GHG emissions and transport prior to dredging operations.

Our conceptual model (Figure 1-1) shows aqueous contaminants infiltrating the subsurface vertically and transported laterally by tile drains and the water table. CO_2 production occurs in organic rich oxygenated soils. CH_4 and N_2O are produced in saturated anaerobic soil bodies.

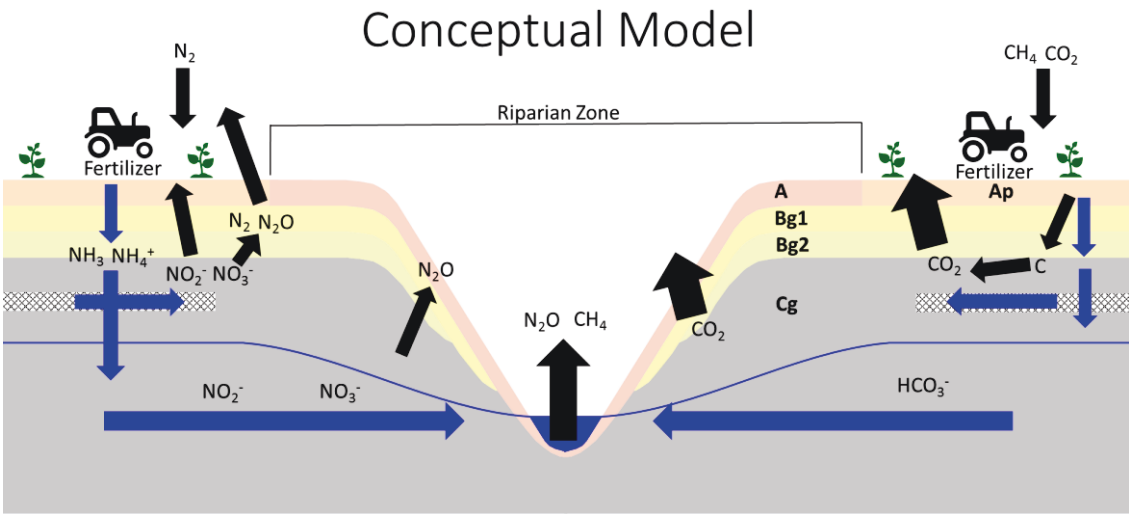

Figure 1-1. Conceptual model of gas and aqueous phase contaminants at our field site. Black arrows show expected gas cycling and blue arrows show aqueous transport (hatched lines are tile drains). The figure is not to scale as the field is larger (~5 ha) than the riparian zone (~0.04 ha).

1.1 References

Ball, B. C. (2013). Soil structure and greenhouse gas emissions: A synthesis of 20 years of experimentation. *European Journal of Soil Science*, *64*(3), 357–373. https://doi.org/10.1111/ejss.12013

Cole, C., Duxbury, J., & Freney, J. (1997). Global estimates of potential mitigation of greenhouse gas emissions by agriculture. *Nutrient Cycling in Agroecosystems*, *49*(1–3), 221–228. https://doi.org/10.1023/A:1009731711346

Duxbury, J. M. (1994). The significance of agricultural sources of greenhouse gases. *Fertilizer Research*, *38*(2), 151–163. https://doi.org/10.1007/BF00748775

ECCC. (2018). *National Inventory Report 1990–2016: Greenhouse Gas Sources and Sinks in Canada*. Retrieved from https://www.canada.ca/en/environment-climate-

Gilliam, J. W., Skaggs, R. W., & Weed, S. B. (1979). Drainage Control to Diminish Nitrate Loss from Agricultural Fields1. *Journal of Environmental Quality*, *8*(1), 137. https://doi.org/10.2134/jeq1979.00472425000800010030x

Gregorich, E. G., Rochette, P., VandenBygaart, A. J., & Angers, D. A. (2005). Greenhouse gas contributions of agricultural soils and potential mitigation practices in Eastern Canada. *Soil and Tillage Research*, *83*(1 SPEC. ISS.), 53–72. https://doi.org/10.1016/j.still.2005.02.009

Nangia, V., Sunohara, M. D., Topp, E., Gregorich, E. G., Drury, C. F., Gottschall, N., & Lapen, D. R. (2013). Measuring and modeling the effects of drainage water management on soil greenhouse gas fluxes from corn and soybean fields. *Journal of Environmental Management*, *129*, 652–664. https://doi.org/10.1016/j.jenvman.2013.05.040

Paustian, K., Lehmann, J., Ogle, S., Reay, D., Robertson, G. P., & Smith, P. (2016). Climate-smart soils. *Nature*, *532*(7597), 49–57. https://doi.org/10.1038/nature17174

Smith, P, Bustamante, M., Ahammad, H., Clark, H., Dong, H., Elsiddig, E. ., et al. (2014). Agriculture, Forestry and Other Land Use (AFOLU). *Climate Change 2014: Mitigation of Climate Change*, 811–922. https://doi.org/10.1017/cbo9781107415416.017

Sunohara, M. D., Craiovan, E., Topp, E., Gottschall, N., Drury, C. F., & Lapen, D. R. (2014). Comprehensive Nitrogen Budgets for Controlled Tile Drainage Fields in Eastern Ontario, Canada. *Journal of Environment Quality*, *43*(2), 617. https://doi.org/10.2134/jeq2013.04.0117

Sunohara, M. D., Gottschall, N., Wilkes, G., Craiovan, E., Topp, E., Que, Z., et al. (2015). Long-Term Observations of Nitrogen and Phosphorus Export in Paired-Agricultural Watersheds under Controlled and Conventional Tile Drainage. *Journal of Environment Quality*, *44*(5), 1589. https://doi.org/10.2134/jeq2015.01.0008

2.0 CH_4, CO_2 and N_2O Production, Consumption and Transport Within Two Controlled Tile Drained Agriculture Fields in Eastern Ontario

2.1 Introduction

Greenhouse gas (GHG) emissions related to agriculture have become a growing concern. Approximately 60-70% of global nitrous oxide (N_2O) and 50% of methane (CH_4) emissions are linked to agriculture activity; however, a large proportion of CH_4 emissions are related to livestock agriculture (Cole et al., 1997; Reay et al., 2012; World Bank Group, 2019). Agriculture soils produce CH_4 when they exhibit anaerobic conditions and replicate wetland environments (Whiting & Chanton, 2001).

Carbon dioxide (CO_2) produces 79% of Canada's emissions but are primarily generated from burning fossil fuels (ECCC, 2018). Even though agriculture is responsible for small contributions to atmospheric CO_2 levels, it has the capacity to influence the carbon budget based on its sink and source capacity (Duxbury, 1994; Gregorich et al., 2005; Tubiello et al., 2015). This is important as agriculture soils have the ability to mediate some of the CO_2 emissions from other industries (Gunter et al., 1998a).

Environmental issues related to GHG cycling are reduced by best management practices (BMPs) which are meant to enhance water quality and reduce GHG emissions. Irrigation management, changes in livestock feed and altering fertilizer application are some examples of agriculture BMPs used today (Cole et al., 1997). Preserving riparian vegetation within agriculture systems is also considered a BMP because its ability to reduce effluent velocity as well as attenuate contaminates (Qi & Altinakar, 2011). This is commonly practiced through drainage ditches which are small streams that reside at the edge of agriculture fields and provide transport pathways for water runoff. This BMP is

effective at reducing nitrogen loading to surface waters but may intensify N_2O emissions due to increased residence time of nitrogen species within the riparian buffer zone (Hefting et al., 2003).

Altering field drainage is another common BMP and implemented by a network of subsurface tiles that divert flow through drainage outlets into drainage ditches (Gilliam et al., 1979; Sunohara et al., 2016). This form of irrigation management is referred to as uncontrolled tile drainage (UCTD) and allows subsurface water transport to occur at a much faster rate than it would through the undrained soil alone. Modern tile drainage systems have been modified to control field tile discharge rates and is referred to as controlled tile drainage (CTD). Control structures are installed near the drainage outlets and are outfitted with flashboard risers which control field water saturation and drainage discharge (Evans et al., 1995).

Numerous studies have shown the effectiveness of CTD as a control on water quality. Nitrogen and phosphorus loading in drainage waters can decrease up to 30% and 50%, respectively, between CTD and UCTD practices (Evans et al., 1995). A mass balance study showed a decrease in nitrogen effluent discharge in CTD systems as they yielded nitrogen losses of 0.01 kg ha^{-1} day^{-1} compared to the 0.02 kg ha^{-1} day^{-1} from UCTD (Sunohara et al., 2014). Sunohara et al. (2016) found that tile water chemistry is similar in both CTD and UCTD systems which suggests that the effectiveness of CTD is directly related to its ability to reduce effluent discharge into drainage ditches.

Overall, CTD is considered a useful BMP due to its effectiveness on enhancing water quality and also proving to have a positive influence on crop production (Crabbé et al., 2012; Ng et al., 2002) making it well received by farmers. However, the effects of CTD may have other environmental impacts such as amplifying GHG emissions. Sunohara et al. (2014) shows that there is a significant increase in nitrogen gas fluxes from CTD when compared to their UCTD counterpart ($P \leq 0.01$ from corn fields & $P \leq 0.06$ from soy fields). In contrast, a similar study found no statistical difference ($P > 0.05$) between GHG emissions from CTD and UTD, but stated that this may be related to the weather conditions during the study period (Van Zandvoort et al., 2017a).

Soil and root respiration are major sources of CO_2 within agriculture soils (Oertel et al., 2016), each having equal contributions to overall production. Respiration rates are dependent on vegetation type but can change based on temporal variations. This can either decrease or increase the contribution of root respiration to net CO_2 production (Hanson et al., 2000). Both processes share the same chemical expression (Stumm & Morgan, 2012);

$$C_6H_{12}O_6 + 6O_2 \rightarrow 6CO_2 + 6H_2O \qquad (2.1)$$

the only difference being soil respiration is driven by microorganisms and root respiration by plant material. The reverse reaction is photosynthesis.

Physical changes within soil horizons can have a substantial influence on CO_2 production. Moisture content is considered to be dominant control on CO_2 fluxes and subsurface concentration profiles as shown through controlled simulations (Hashimoto & Komatsu, 2006). Schaufler et al., (2010) states that 40% water saturation is ideal

conditions for CO_2 production. Over or under saturated soils can drastically decrease production rates due to the scarce supply of oxygen or inadequate environment for respiration (2.1) to proceed (Moncrieff & Fang, 1999). Infield observations have proven challenging to quantify the relationship between CO_2 emissions and moisture content (Van Zandvoort et al., 2017b), but some correlation is observed (r^2 = 0.26; Mielnick & Dugas, 2000).

Temperature variations can have a greater influence on field CO_2 fluxes than moisture content (Moncrieff & Fang, 1999; Nangia et al., 2013). A controlled laboratory study showed that there is an exponential increase in CO_2 production when temperatures exceed 10 ^oC (Fierer et al., 2003). Hashimoto & Komatsu (2006) also state that temperature elevates soil CO_2 concentrations as well as amplifying surface CO_2 fluxes.

The ability for these systems to produce or consume CH_4 is defined by two processes, methanogenesis and methanotrophy (Dutaur & Verchot, 2007). Methanogenesis is the anaerobic production of methane;

$$CO_2 + 4H_2 \rightarrow CH_4 + 2H_2O \qquad (2.2)$$

as methanogens metabolize carbon complexes such as CO_2 (Duxbury, 1994; Topp & Pattey, 2011). This is common in wetlands where high rates of carbon fixation are linked to greater CH_4 emissions due to higher production rates (Whiting & Chanton, 1993).

Methane oxidation (methanotrophy) is a microbial driven reaction that consumes CH_4 to produce CO_2 (Dutaur & Verchot, 2007);

$$CH_4 + 4O_2 \rightarrow CO_2 + 2H_2O \quad (2.3)$$

Upper soil horizons act as diffusive pathways for atmospheric CH_4 which is then consumed by microbes in aerobic soil layers (Prather et al., 1995). Disturbing the oxidizing surface soil horizons through tillage can reduce CH_4 oxidation rates by agitating oxidizing microbes (Ball et al., 1999). Tillage can also influence physical soil properties like porosity which can alter CH_4 influx diffusive pathways, reducing the availability of CH_4 for oxidation reactions (2.3) to proceed (Ball et al., 1999).

Nitrous oxide emissions are produced as a series of microbial driven reactions. Nitrification is the oxidizing reaction of nitrogen complexes such as ammonium (NH_4^+) and ammonia (NH_3) which produce nitrite (NO_2^-) which is then oxidized to nitrate (NO_3^-) (Stumm & Morgan, 2012);

$$NH_4^+ + \tfrac{3}{2}O_2 \rightarrow NO_2^- + H_2O + 2H^+ \quad (2.4)$$

$$NH_3 + O_2 \rightarrow NO_2^- + 3H^+ \quad (2.5)$$

$$NO_2^- + \tfrac{1}{2}O_2 \rightarrow NO_3^- \quad (2.6)$$

In agriculture systems, these nitrifying pathways are linked to fertilizer applications (Duxbury, 1994). Nitrate will move through the subsurface until it is reduced by denitrifying bacteria and produce N_2O and nitrogen gas (N_2; Smith et al., 2018);

$$NO_3^- \rightarrow NO_2^- \rightarrow NO \rightarrow N_2O \rightarrow N_2 \quad (2.7)$$

Nitrous oxide is a dominant product of denitrification in oxygen depleted, saturated environments (Davidson et al., 2000) but nitric oxide (NO) is a common gas product in oxygenated soil zones (Russow et al., 2000). This shows that the fate of nitrogen speciation pathways are controlled by subsurface soil properties (Schaufler et al., 2010).

Changes in oxidation rates and moisture content are dominant controls on denitrifying pathways and regulate N_2O production (Ball, 2013). Pihlatie et al. (2004) show that increasing water saturation can increase N_2O production by four orders of magnitude. Soils will produce highest levels of N_2O when water saturation is $\geq 60\%$ which is when micropores are saturated and permit microbes to breakdown NO_3^- due to the anaerobic conditions (Davidson et al., 2000).

Heterogeneity within the subsurface can cause spatial irregularities in N_2O production due to pockets of anaerobic regions called hotspots (Gregorich et al., 2005). Hot spots are small, localized regions where denitrification is amplified, creating isolated areas of high N_2O production. They are caused by pockets of organic matter in regions with poor diffusive properties (Ambus & Christensen, 1994). Tillage can influence the distribution of organic material and cause heterogeneity to the subsurface diffusive profile (Ball, 2013).

2.1.1 Purpose

This work aims to define the transport mechanisms that are responsible for gas migration within an experimental watershed in Eastern Ontario. This will help to understand the controls on spatially and temporally variable gas transport and develop predictive models of the impact of natural and anthropogenic changes on gas emissions and effluent contaminant fluxes. A quality predictive model is useful in developing best management practices (BMPs) to reduce the environmental impacts associated with agricultural activity

2.2 Site Description

This study was conducted on privately owned agricultural lands within the South Nation Watershed located Southeast of Ottawa (Figure 2-1A). The study site was designated as an experimental watershed for the Watershed Evaluation of Beneficial Management Practices (WEBs) project from 2004 to 2013 and has been used since to conduct other AAFC experimental work such as the AGGP. AAFC has divided WEBs into numerous sites for varying research purposes. This study focuses on two sites, 1 and 10 (Figure 2-1B). Both are characterized as CTD systems and are on the same crop rotation; corn fields in 2017 and soya fields in 2018. The two sites vary based on riparian zone vegetation (Table 2-1). Site 1 is classified as a grassy microecosystem and site 10 is dominated by larger shrubs and small trees. However, they both contain a high density of Smooth Bromegrass (South Nation Conservation, 2017). The stream and bank at site 10 are shaded due to the larger plant species.

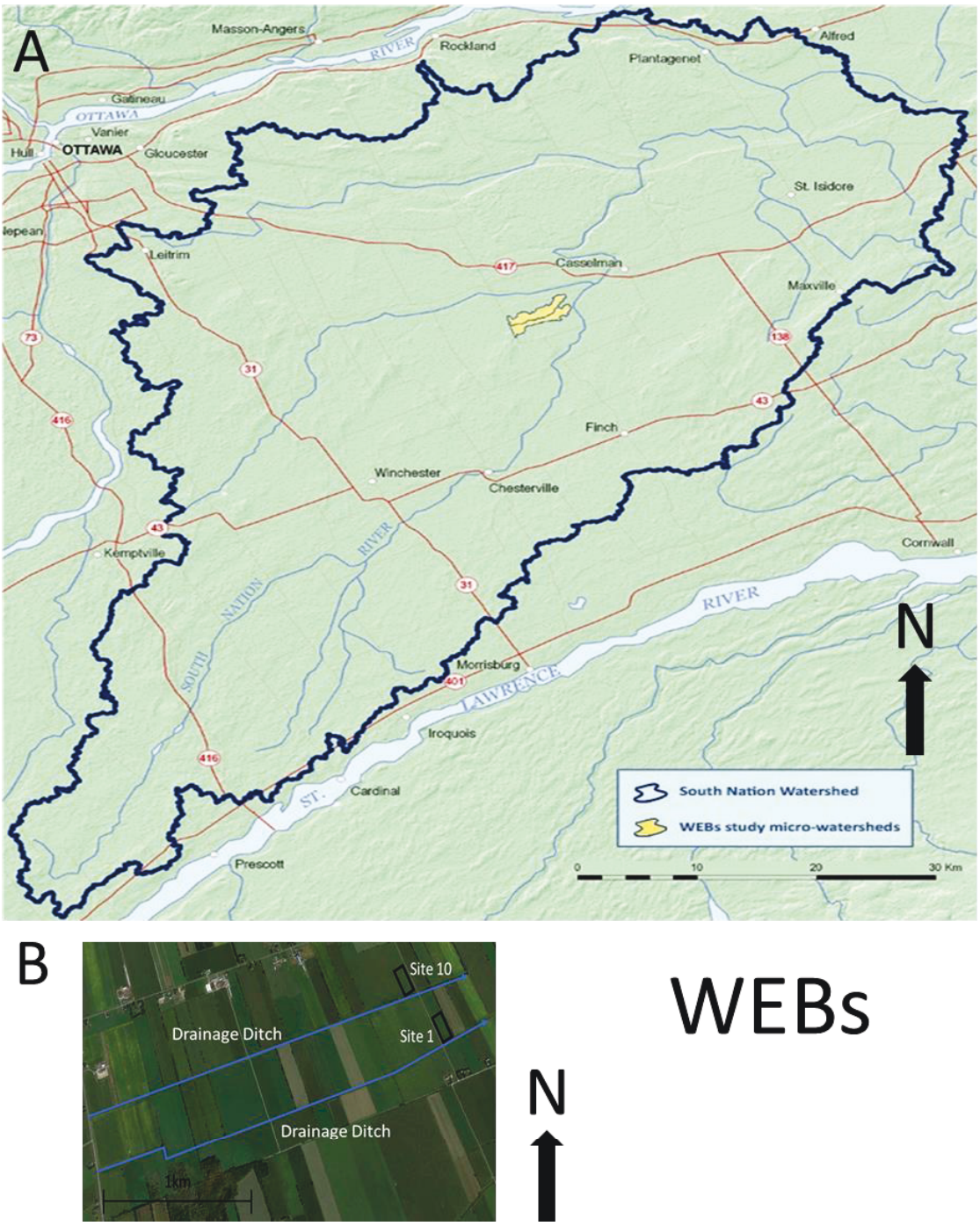

Figure 2-1. A) The South Nation Watershed is outlined by the blue border and contains the WEBs experimental watershed (Agriculture and Agri-Food Canada, 2013). B) The two field sites are outlined and fall within the WEBs watershed. Each site drains into a separate drainage ditch (Modified from Google Earth, 2019).

Site	Riparian Vegetation
1	Bittersweet Nightshade, Butter and Eggs, Common Burdock, Common Dandelion, Common Milkweed, Vicia cracca, Curly Dock, Field Horsetail Grass, Goat's Beard, Lady's Thumb spp., Purple loosestrife, Red Osier Dogwood, Sweet Goldenrod, Wild Parsnip, Yellow Rocket
10	Willow spp., Bindweed, Black Night shade, Canada Thistle, Common Cattail, Common Tansy, Cow Vetch, Field Horsetail Grass, Green Amaranth, Manitoba Maple, New England Aster, Nodding Foxtail, Northern Water Plantain, Penciled Aster, Purple Lossetrife, Red Clover, Red Osier Dogwood, Rice Cutgrass, Sow Thistle, Spotted Jewelweed, Sweet Goldenrod, White Ash, Wild Carrot, Wild Cucumber, Wild Raspberries, Yellow Rocket

Table 2-1. List of vegetation species found within the riparian zones of sites 1 and 10 (South Nation Conservation, 2017).

The study sites reside on a Bainsville soil series (Wicklund & Richards, 1962a). The soils are derived from marine deposits (Government of Canada, 2013; Wicklund & Richards, 1962b) which create a succession of clay and silty sands (Table 2-2). The series is poorly drained which gives them a darker appearance than similar soils in surrounding regions (Wicklund & Richards, 1962b). The Ap horizon is rich in organics and is altered due to agricultural activity. Bg1 and Bg2 are similar and characterized by fine sands and silts. The basement horizon, Cg, is dominated by clay and has poor hydraulic conductivity (Schut & Wilson, 1987; Wicklund & Richards, 1962b). The suffix “g” is used to describe the gleying properties of the soil horizons (Agriculture and Agri-Food Canada, 1998)

Horizon	Depth (cm)	Organic Matter%	Sand%	Silt%	Clay%	K (cm/h)	BD (g/cm^3)
Ap	0-22	5.5	44	44	12	2.5	1.29
Bg1	22-37	0.3	64	34	2	1.2	1.49
Bg2	37-49	0.1	40	45	15	3.8	1.53
Cg	49-100	0.3	8	44	48	N/A	1.47

Table 2-2. Four horizons of the Bainsville series defined by Schut & Wilson (1987). K is hydraulic conductivity and BD defines bulk density. The series is variable throughout the field area due to heterogeneity but shows a similar profile overall.

These sites are tile drained systems (Figure 2-2). Tiles are 102 mm perforated corrugated plastic pipes that sit 1 m subsurface and spaced 15 m apart (Sunohara et al., 2015). They run parallel to each other and have a shallow gradient of 0.1% which allows drainage to flow towards a collection header. The header tile (152 mm diameter perforated corrugated plastic pipe) diverts flow through two drainage outlets and into a drainage ditch (Gilliam et al., 1979; Sunohara et al., 2015). The header is located approximately 15 m from the edge of the field (Sunohara et al., 2016).

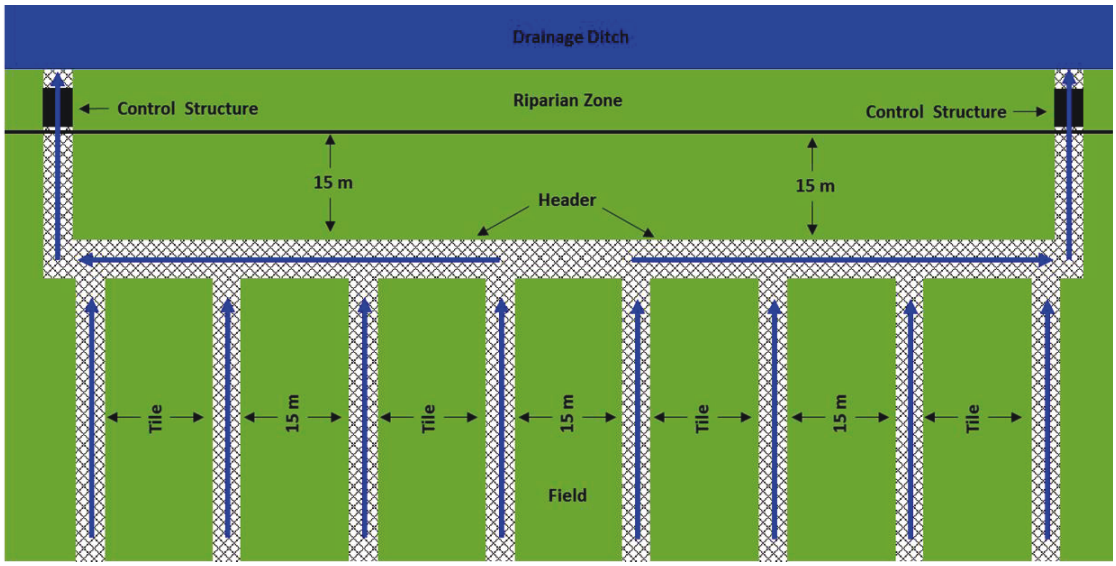

Figure 2-2. Tile drains run parallel to each other and direct flow into a collection header tile. The header diverts flow towards control structures where drainage outlets discharge effluent into the drainage ditch.

2.3 Methods

This field study used numerous field sampling techniques to characterize physical and geochemical properties and processes within the agricultural fields and riparian zones. Sampling locations are positioned in the field, shoulder, bank and stream at both sites (Figure 2-3). Greenhouse gas and Li-COR chambers were located at all field, shoulder and bank locations. Surface gas chambers were used to measure changes in surface gas concentrations to calculate a gas flux. Li-COR chambers were used to measure direct CO_2 fluxes in the field. The eastern sampling locations contained additional equipment which included, suction lysimeters, piezometers and gas sampling rods. Unsaturated zone water samples were collected by the suction lysimeters and water table samples were taken using piezometers. Subsurface gas concentrations were measured using the nest of gas sampling rods. The field location was 10 m from the shoulder. The shoulder was the region between the edge of the farm field and the bank of the drainage ditch. The shoulder contained a thermocouple nest used to measure soil temperature profiles and control structures used to collect tile effluent samples. The shoulder was approximately 1 m in width. The banks are generally steep, leading to the stream approximately 2 m below the field. ISCO autosamplers were used to collect stream water samples.

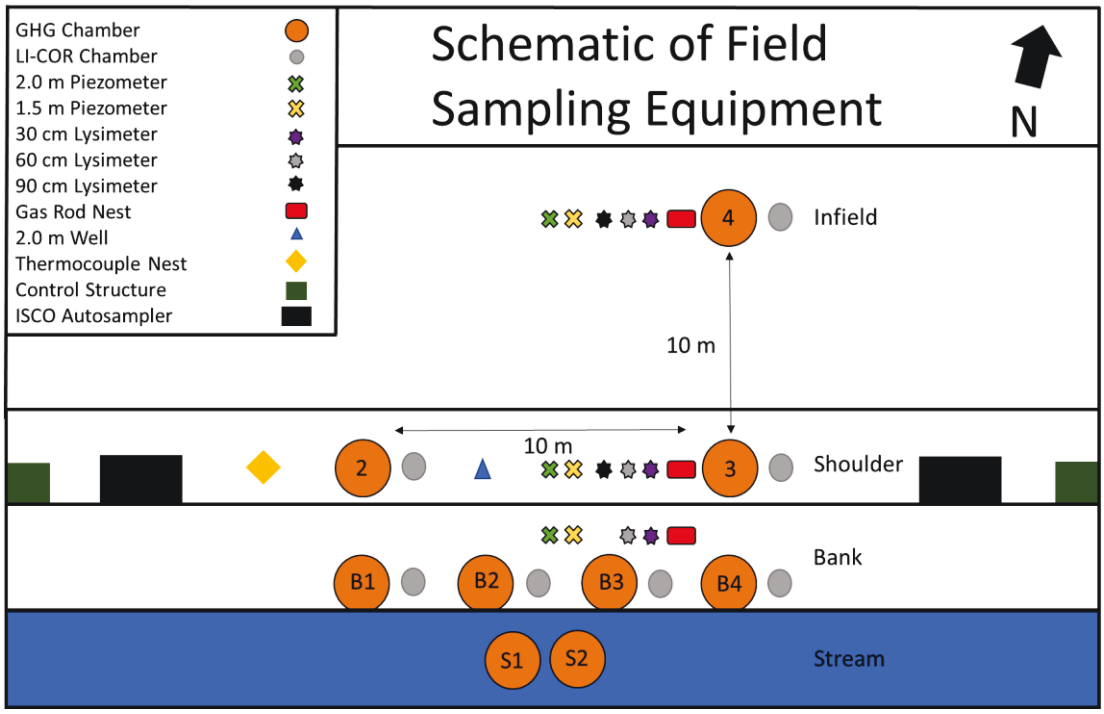

Figure 2-3. Schematic of field sampling equipment at sites 1 and 10

This study focused on a sampling transect that ran perpendicular to the 4, 3, B3 and B4 sampling locations. The transect included three nests of sampling equipment that penetrated a variety of subsurface horizons (Figure 2-4). The sampling equipment were actually located in a line perpendicular to the sampling transect (Figure 2-3), but are shown in line with the sampling transect in Figure 2-4 to show a cross-section.

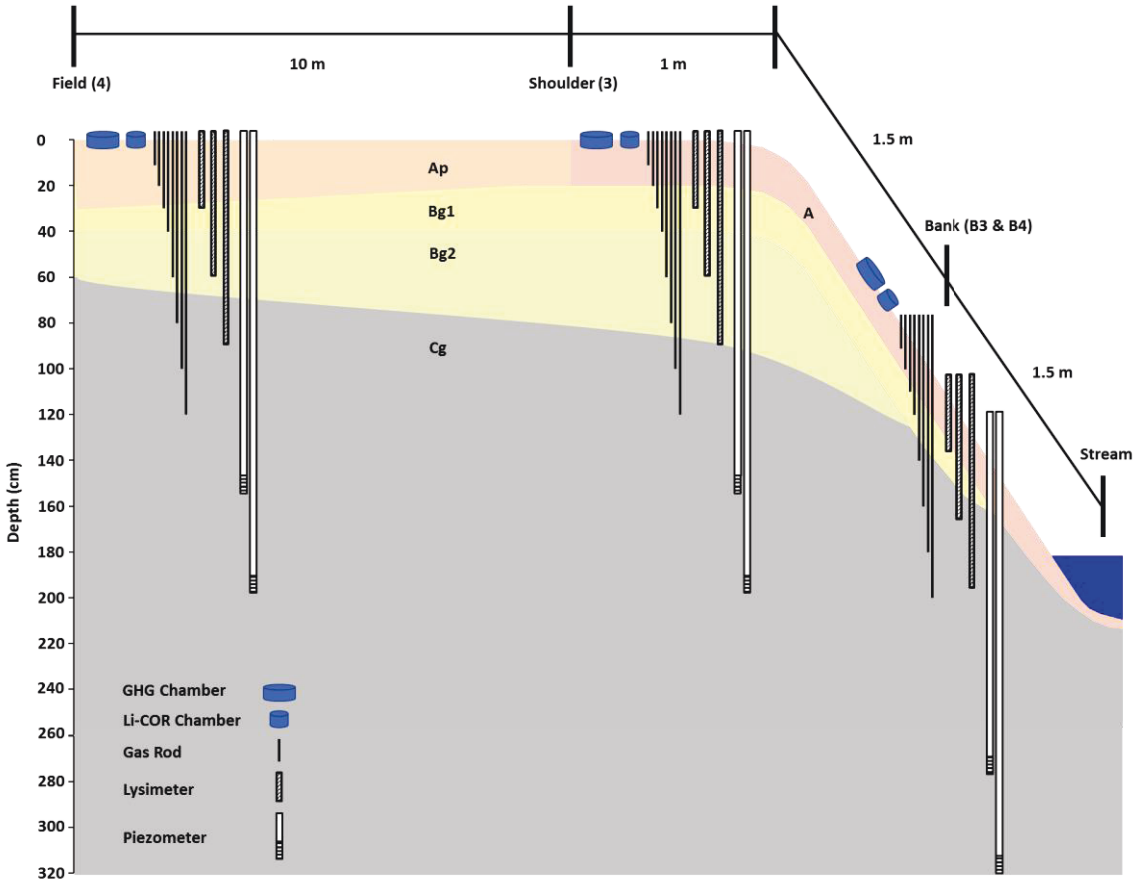

Figure 2-4. Sampling equipment used in this study was positioned along a transect that ran perpendicular through the field, shoulder and bank. The soil horizons were determined by physical and geochemical properties from soil cores collected during this study and previous soil surveys (Schut & Wilson, 1987; Wicklund & Richards, 1962b).

Two types of gas sampling methods were conducted; surface flux and subsurface gas measurements. Surface fluxes were measured employing a non-steady state technique using gas chambers to measure changes in GHG concentrations over time (Rochette & Bertrand, 2008; Rochette & Hutchinson, 2005). Subsurface gas concentrations were measured from ¼" stainless steel rods that were installed at sampling depths from 10 cm to 120 cm (gradient method; Kusa et al., 2008; M. Maier & Schack-Kirchner, 2014).

2.3.1.1 Surface Fluxes

Gas chambers were constructed from 36 cm diameter by 20 cm high PVC pipe (EMCO Waterworks) and 19 cm diameter by 15 cm high PVC pipe (EMCO Waterworks). They were tampered 10-15 cm into the soil at the sampling locations specified in Figure 2-3. Larger chambers were used for surface flux measurements and the smaller chambers for LiCOR CO_2 flux measurements. The chambers were installed in May and remained in the soil for the agronomic season.

For the larger chambers, five gas samples were collected from each chamber for flux measurements. An initial sample was collected from the open chamber then a 36 cm diameter by 5 cm high PVC pipe lid was placed on top of the open chamber to allow gas to accumulate for future samples. Four more samples were taken every five minutes over a 20-minute interval after the chambers were closed. A rubber septum stopper was used as an access port to draw samples from the closed chambers. A 30 mL syringe was used to draw the gas sample and inject it into a 12 mL Labco Exetainer vial. The samples were sent to AAFC and analyzed on an Agilent 7890B gas chromatograph for GHG concentrations.

A surface gas flux was calculated by Doucet (2019) using the change in concentration over time $(\partial c/\partial t)$ for each gas chamber ever week using the equation (Rochette & Bertrand, 2008);

$$J_{sur,i} = \frac{\partial c}{\partial t} M_{mg} / (V_m \, (1 - \frac{e_p}{p}) \qquad (2.8)$$

where $J_{sur,i}$ is the mass flux of the desired analyte i (g m^{-2} s^{-1}). A is the gas emitting

surface area, M_m is the gram formula weight of the analyte (g), V_m is the air volume based on chamber pressure and temperature conditions, and e_p is the relative humidity within the chamber. Only $\partial c/\partial t$ values with a r^2 value of ≥ 0.9 are used for surface flux calculations.

A Li-COR LI-8100A CO_2 flux analyzer was also used to measure CO_2 surface fluxes. The 20 cm Li-COR survey chamber was placed on the LiCOR flux chamber (19 cm diameter) and recorded a real-time flux over a two-minute interval.

2.3.1.2 Subsurface Gas Samples

Stainless steel sampling rods ¼" in diameter were installed next to a bank (B3 and B4), shoulder (3) and field (4) surface chamber (Figure 2-3). An inner installation rod was used to hammer the rods to their desired depths of 10 cm, 20 cm, 30 cm, 40 cm, 60 cm, 80 cm, 100 cm and 120 cm, then removed. The rods were installed at the beginning of the field season (May) and remained onsite throughout the agronomic season.

Each rod was sampled approximately every week using a 30-60 mL syringe and luer lock 40 cm long tubbing attachment. The tubbing attachment was used to connect the luer lock to the gas rods. A minimum of one rod volume of gas was purged prior drawing a sample. The samples were injected into a 12mL Exetainer. Saturated soil horizons sometimes limited the number of rods sampled. Rod samples were analyzed at Carleton University on a SRI 8610C gas chromatograph.

Subsurface gas samples were used to calculate a subsurface diffusive flux based on Fick's first law (Mayer et al., 2002);

$$J_{sub,i} = -D_i S_g T_g \varphi \frac{\partial c}{\partial z} \quad (2.9)$$

The subsurface mass flux for gas i ($J_{sub,i}$) is reported as g m^{-2} s^{-1} and calculated based on the diffusion coefficient of the specific analyte in air (D_i), gas phase saturation (S_g), tortuosity (T_g), porosity (φ) and the concentration gradient ($\partial c/\partial z$). Diffusion coefficients were taken from the Handbook of Chemistry and Physics and reflect the diffusivity of the specific analyte in an excess of air at 20 °C (CO_2 0.160 cm^2 s^{-1} and CH_4 0.210 cm^2 s^{-1}; Rumble, 2018). The diffusion coefficient for CO_2 was used for N_2O as they behave similarly (Kusa et al., 2008). Aqueous phase water saturation (S_a) was determined using infield moisture content measurements (θ) and porosity which were then used to calculate a gas phase saturation term (Mayer et al., 2002);

$$S_g = 1 - S_a \qquad (S_a = \frac{\theta}{\varphi}) \quad (2.10)$$

Tortuosity was calculated based on porosity and gas phase saturation (Millington, 1959);

$$T_g = {S_g}^{7/3} \varphi^{1/3} \quad (2.11)$$

Moisture content measurements were collected from Moisture Point probes (15 cm, 30 cm, 45 cm, 60 cm, 90 cm in the field and shoulder; 20 cm in the bank) and assigned to gas rod measurements at those depths to calculate S_a and S_g. In the field and shoulder, when moisture content measurements were taken at a different depth than the gas rods, the 15 cm θ values were assigned to the 10 cm and 20 cm gas rods, the 45 cm θ values to 40 cm gas rods and 90 cm θ values to 80 cm, 100 cm and 120 cm gas rods. In the bank, 20 cm θ values were assigned to the 10 cm, 20 cm and 30 cm gas rods. The deeper samples (≥ 40 cm depth) were assigned a moisture content value of 45% based on qualitative observations of near saturated soils at those depths. Porosity values were taken

from AAFC moisture retention curves that were constructed from Bainsville soil samples. Porosity values were 0.53 for the Ap/A horizon, 0.51 for the Bg1 horizon and 0.50 for the Bg2 and Cg horizon.

For each term used in Eq 2.9, a value was determined for each rod depth. Those terms where averaged over eight intervals (0-10 cm, 10-20 cm, 20-30 cm 30-40 cm, 40-60 cm, 60-80 cm, 80-100 cm and 100-120 cm) and used to calculate a mass flux using the concentration gradients over those intervals. The calculated fluxes were averaged over three intervals (0-20 cm, 20-40 cm, 40-120 cm) and are reported at the lowest depth of the flux interval.

2.3.1.3 CO_2 Production

Guitard (2019) conducted an experiment to determine CO_2 production rates at WEBs. Intact soil cores (3" diameter) were collected from each sampling location at site 1. The cores were collected at 7.5 cm depth intervals and stored in sealed IsoJar containers. Headspace gas samples from the IsoJars were collected over four months and analyzed for CO_2 concentrations. Production rates were calculated using the mass of the core and the change in headspace concentrations over sampling intervals ($\partial c/\partial t$).

2.3.2 Soil Samples

Monthly soils samples were collected using a JMC N-2 handle PN003 soil sampler at each sampling location (field, shoulder, bank) at two depth intervals (0-15 cm and 15-30 cm). A set of augered cores (2.5" diameter) were collected on August 7th, 2018 at each

sampling location at four depth intervals (0-15 cm, 15-40 cm, 40-65 cm and 65-90 cm). All samples were analyzed for nutrients, total Kjeldahl nitrogen (TKN) and carbon content (TC, TOC, TIC). These analyses were conducted at AAFC. Nutrients and TKN analyses were conducted on a Lachat QuikChem 8500 Series 2 Flow Injection Analysis System using a KCl extraction (method 12-107-04-1-B) and a Kjeldahl digestion (method 13-107-06-2-D) respectively. Carbon analyses were conducted on a LECO CR-12 Carbon System (781-600).

The augered core samples were analyzed at the Agriculture and Food Laboratory (University of Guelph) for particle size distribution (method SNL-022), cation exchange capacity (CEC; method SNL-034) and organic matter (method SNL-027).

2.3.3 Water Samples

Monthly samples were collected during the 2018 field season from piezometers, lysimeters, control structures and the drainage ditches. Samples were analyzed on site for pH, ORP, EC, NH_3-N, PO_4^{3-} and alkalinity. Samples were split onsite for dissolved inorganic carbon (DIC), dissolved organic carbon (DOC), cation and anion analyses, which were conducted at the University of Waterloo.

Piezometers and lysimeters were installed at three sampling locations at each field site (Figure 2-3 and Figure 2-4). Each piece of sampling equipment was outfitted with dedicated ¼" polyethylene tubbing for sample extraction.

Drive point piezometers were constructed from 1.5” PVC pipe and have a 15 cm screen (40 μm porous tube). A 50 cm deep hole was augered at the installation locations and the piezometers were placed into holes and jackhammered into the subsurface until they reached desired depths (150 cm and 200 cm). Silica sand was used to backfill around the screen then bentonite backfilled most of the remaining of the hole. The top of the hole was backfilled using parent site material.

Suction lysimeters (Soil Moisture Equipment Corp, model 1900L) were installed at the same transect locations as the piezometers. Lysimeters were made of 1.8” diameter PVC pipe with a porous ceramic cup. A hole was augured to the desired installation depth (30 cm, 60 cm and 90 cm). The augured material was mixed with water to create a backfill slurry which backfilled the space around the ceramic cup. Remnant augered soil was used to backfill the rest of the hole. Model 1900L24-BO2M2 (24”) was used for 30 cm sampling depths and a 1900L36-BO2M2 (36”) was used for 60 cm and 90 cm sampling depths.

A VWR symphony H30PCO meter and 89231-656 probe was used to measure pH, ORP, EC and temperature. Calibrations were conducted daily using pH 4, 7 and 10 buffer solutions, Zobel’s solution for ORP, 1410 μS and 12.9 mS EC standards. Alkalinity was analyzed using a digital titrator as specified by Hach method 8203 (HACH, 2018). NH_3-N and PO_4^{3-} were both analyzed on a HACH 1900 spectrophotometer using methods 10023 (HACH, 2015) and 8048 (HACH, 2017), respectively.

A 125 mL amber polyethylene sample bottle was used to collect water samples that were drawn using a peristaltic pump. Due to limited water availability, piezometers and lysimeters were purged after samples were collected and allowed to refill for the next sampling period.

All samples for laboratory analysis were filtered using a cellulose acetate 45 μm filter. DOC samples were preserved with 3 N H_2SO_4 (pH < 2) and cation samples were preserved with 3 N HNO_3 (pH < 2). DOC and cation samples were refrigerated during storage. Anion and DIC samples were not acidified but frozen for preservation. All samples were sent to UW for analysis. DOC and DIC samples were analyzed on an Aurora 1030W TOC Analyser (TOC_CP_Jan 15_2015). Cations were analyzed on a Thermo Fisher ICAP 6000 (ICP-OES) and a Thermo Fisher XSERIES 2 (ICP-MS). A Dionex IC-CO3 System (ion exchange chromatography) was used for anion analysis.

2.4 Results

2.4.1 Gas Data

Subsurface CH_4 concentrations from sites 1 and 10 show a decrease from atmospheric concentrations (mean of 1.95 ppm) to values as low as 5.00×10^{-1} ppm with depth (Figure 2-5). There is minimal spatial variation in the CH_4 concentration profiles throughout the sampling transects; however, it is apparent that the profiles do show temporal variability at each sampling location. Some sample dates show a steady decrease in CH_4 concentrations where others show fluctuation within an overall decreasing trend. At site 10, most profiles show a steep gradient near the surface (0-40 cm) with a shallower gradient at greater depths. Even though most of the profiles agree with this trend, they show very different concentration ranges. The site 1 profiles are similar to site 10 but show more of a consistent gradient from surface to depth. Those consistent gradients still vary temporally as they also range from atmospheric values to 1 ppm on some days where others range from atmospheric values to below 5.00×10^{-1} ppm. Both sites consist of a few profiles that disagree with the decreasing concentration trend and show values that stay close to atmospheric levels at depth. It is common to observe some noise within the profiles due to heterogeneity and temporal variability, but the noise may also be amplified due to the sensitivity of the CH_4 analytical measurements.

Carbon dioxide is observed to increase with depth. Lowest values are found at surface and resemble atmospheric CO_2 concentrations (mean of 422 ppm; Figure 2-5). Highest concentrations are seen at 60 cm and below and can reach values upwards of

30000 ppm. Spatial trends are evident at both sites 1 and 10 as CO_2 concentration maximums are higher in the field (30000-43000 ppm at site 1 and 24000-28000 ppm at site 10) than in the bank (10000-15000 ppm at site 1 and 16000-19000 ppm at site 10). Although both sites show similar trends, there are still some noticeable differences between the two site profiles. Site 10 field and shoulder CO_2 profiles show a steeper concentration gradient above 60 cm than below. Concentrations seem to plateau below 60 cm thus remaining consistent at greater depths. The site 1 field profile also shows a steep gradient from the surface to 60 cm, but the limited data set doesn't provide enough data below 60 cm to distinguish trends. The site 1 shoulder profile shows different trends than the site 10 shoulder. Both sites exhibit steeper concentration gradients between 0-40 cm; however, most site 1 profiles show a decrease in CO_2 concentrations below 40 cm before increasing again back to their maximum values at 80-100 cm. The site 10 shoulder concentrations remain close to maximum values below 40 cm. Both sites show temporal variations as each individual profile shows unique maximum and minimum values; however, they seem to resemble similar trends within each sampling location. There is approximately 10000-15000 ppm variability within concentration measurements. The site 1 field profiles show the greatest variability with a 30000 ppm difference between minimum and maximum values.

Nitrous oxide depth profiles resemble CO_2 trends as they also increase with depth and change spatially, although N_2O concentrations are much lower than CO_2 values (Figure 2-5). Atmospheric concentrations (mean of 0.3 ppm) are observed at the surface and are the lowest values in the N_2O profiles. Site 1 has the highest N_2O concentrations

as the field profile shows concentrations approaching 8 ppm. Concentrations are lower in the shoulder with most concentrations ranging between 0.4-1 ppm with a maximum of 3 ppm. Lowest concentrations are observed in the bank with a maximum value of 2.3 ppm and most values falling between 0.4-0.7 ppm. Site 10 shows a similar trend, but the highest concentrations are lower than site 1 reaching values of 4.4 ppm in the field. There are values approaching 4 ppm in the shoulder profile but overall, the shoulder shows lower N_2O concentrations than the field with most values falling between 0.5-1.0 ppm with a maximum of 3.9 ppm. The lowest concentrations are seen at the bank and generally fall between 0.3-0.6 ppm with a maximum of 1.5 ppm. The site 10 field profiles are similar between N_2O and CO_2. Nitrous oxide hits a peak concentration between 40-80 cm then plateaus or decreases with depth. The N_2O profiles also show temporal variability. Just like the CO_2 profiles, each sampling location shows a wide range of maximum values with the greatest disparity observed in the site 1 60 cm field values (0.7-7.5 ppm). Most of the other sampling concentration profiles show approximately 1 ppm variation between minimum and maximum values. In general, the weeks with higher maximums generally have higher overall concentrations which create smooth profiles like CO_2, which limits the amount of noise observed within the profiles.

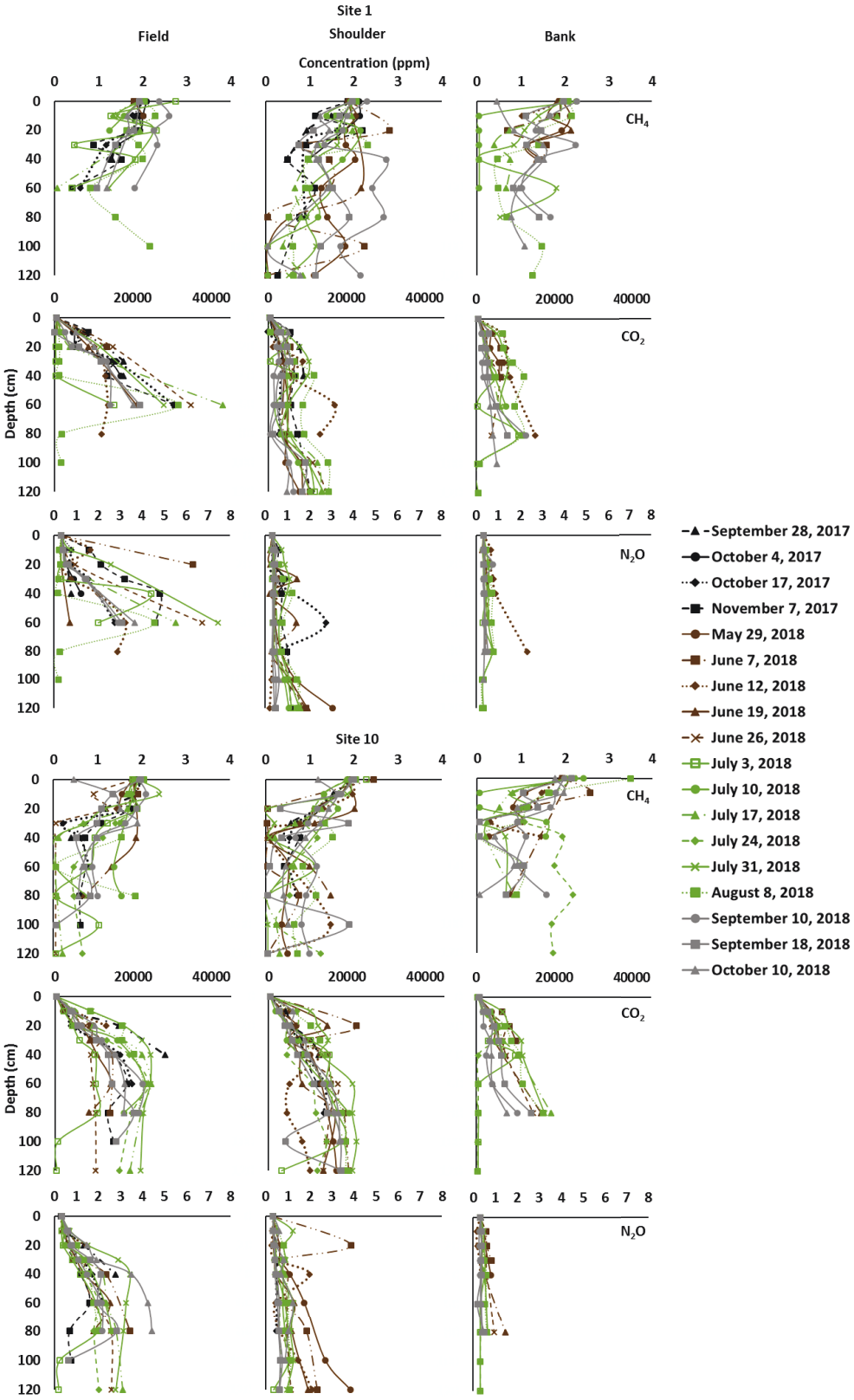

Figure 2-5. Gas concentration profiles from sites 1 and 10. The plots show changes in gas concentrations through the 2017 fall and the 2018 agronomic season. CH_4 concentrations decrease with depth while CO_2 and N_2O concentrations increase with depth.

Surface GHG fluxes throughout the 2018 agronomic season at both sites 1 and 10 show a positive flux of CO_2 and N_2O (efflux; Figure 2-6; Doucet, 2019). Methane is observed as both an efflux (out of the system) and influx (into the system) depending on the location and site (Doucet, 2019). Negative methane fluxes (influx) are observed at all sampling locations at site 1 and the shoulder at site 10. However, the site 10 bank produces a CH_4 efflux. Methane fluxes range between -1.1×10^{-3} to -1.1×10^{-2} to kg ha^{-1} day^{-1} at site 1 and -9.2×10^{-3} to 2.9×10^{-2} kg ha^{-1} day^{-1} at site 10 where nitrous oxide fluxes range between 9.4×10^{-4} to 5.7×10^{-2} kg ha^{-1} day^{-1} at site 1 and 4.9×10^{-4} to 2.8×10^{-2} kg ha^{-1} day^{-1} at site 10. Methane and N_2O fluxes are similar in magnitude in contrast to CO_2 which produces surface fluxes up to five orders of magnitude larger (1.5×10^{1} to 6.6×10^{2} kg ha^{-1} day^{-1} at site 1 and 2.9×10^{1} to 2.9×10^{2} kg ha^{-1} day^{-1} at site 10). There are minimal temporal trends in N_2O and CH_4 fluxes, whereas CO_2 shows a decrease in emissions throughout the agronomic season. There is a peak in N_2O fluxes observed in the field at Site 1 between July 24th and August 8th with values approaching 6.0×10^{-2} kg ha^{-1} day^{-1}.

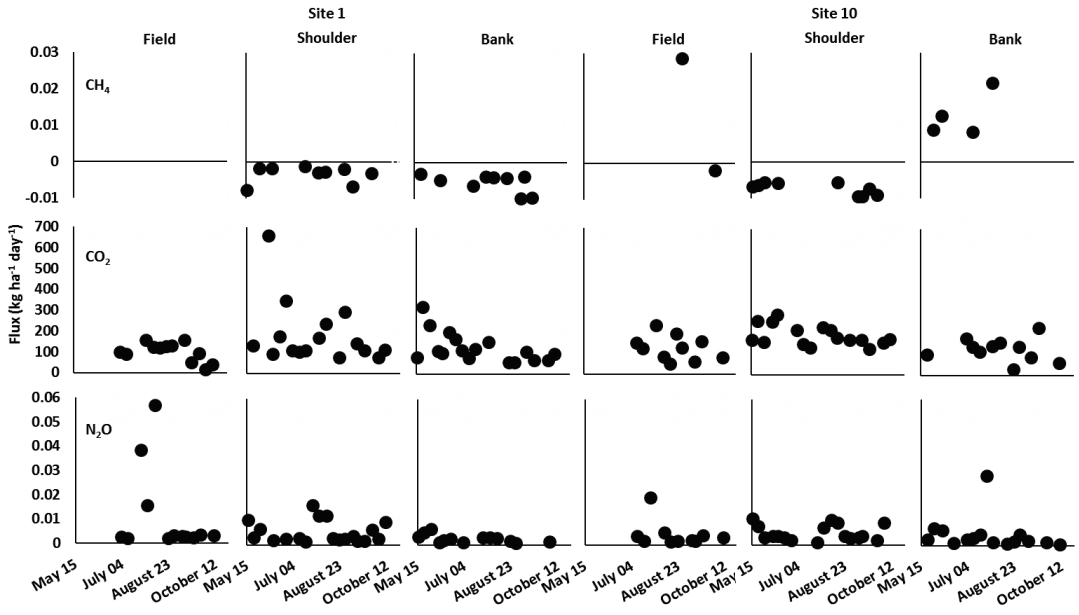

Figure 2-6. Time series of 2018 GHG surface fluxes from both sites. CH_4 and N_2O fluxes are values from the surface gas chamber method and the CO_2 fluxes are from the LiCOR method.

There are minimal spatial differences between GHG surface fluxes throughout the sampling transects and between each site (Figure 2-7). A one-way ANOVA test and a TukeyHSD test is used to determine if there is variability throughout the sites transect while a Welch two sample t-test is used to determine the relationship between identical sampling locations between the two sites (p-value < 0.05 is significant). Methane fluxes are similar at the two sampling locations at site 1 with mean flux values of -4.0×10^{-3} kg ha^{-1} day^{-1} at the shoulder and -5.4×10^{-3} kg ha^{-1} day^{-1} at the bank ($P = 0.32$). There is a poor regression ($r^2 < 0.9$) with all surface chamber site 1 CH_4 field concentration measurements within each sampling period, therefor no fluxes are calculated at that location. There is a difference between site 10 methane values ($P < 0.01$) as mean fluxes are -7.2×10^{-3} kg ha^{-1} day^{-1} at the shoulder and 1.3×10^{-2} kg ha^{-1} day^{-1} at the bank. No mean field CH_4 flux is reported at site 10 due to the limited number of reliable surface flux values and their contrasting fluxes (2.9×10^{-2} kg ha^{-1} day^{-1} and -2.0×10^{-2} kg ha^{-1}

day^{-1}). Site 1 has similar CO_2 fluxes throughout the transect with mean values of 1.0 x 10^2 kg ha^{-1} day^{-1} at the field, 1.8 x 10^2 kg ha^{-1} day^{-1} at the shoulder and 1.3 x 10^2 kg ha^{-1} day^{-1} at the bank (P=0.10). Carbon dioxide surface fluxes show spatial variation at site 10 with the shoulder having higher fluxes (mean of 1.9 x 10^2 kg ha^{-1} day^{-1}) than the field (mean of 1.2 x 10^2 kg ha^{-1} day^{-1} and the bank (mean of 1.2 x 10^2 kg ha^{-1} day^{-1}; $P < 0.01$). Both sites show no significant variation in N_2O surface fluxes within the sampling transects. The mean site 1 values are 1.1 x 10^{-2} kg ha^{-1} day^{-1} at the field, 5.3 x 10^{-3} kg ha^{-1} day^{-1} at the shoulder and 2.8 x 10^{-3} kg ha^{-1} day^{-1} at the bank ($P = 0.11$). Site 10 values are similar with mean N_2O fluxes of 5.1 x 10^{-3} kg ha^{-1} day^{-1} at the field, 5.0 x 10^{-3} kg ha^{-1} day^{-1} at the shoulder and 4.6 x 10^{-3} kg ha^{-1} day^{-1} at the bank.

There are no significant differences between site 1 and 10 CO_2 and N_2O field fluxes ($P = 0.35$ for CO_2 and $P = 0.27$ for N_2O), shoulder fluxes ($P = 0.82$ for CO_2 and $P = 0.79$ for N_2O) and bank fluxes ($P = 0.75$ for CO_2 and $P = 0.35$ for N_2O). Methane shows significant differences between the two sites ($P = 0.02$ at the shoulder and $P < 0.01$ at the bank). There isn't enough CH_4 data to conduct a statistical analysis regarding field fluxes.

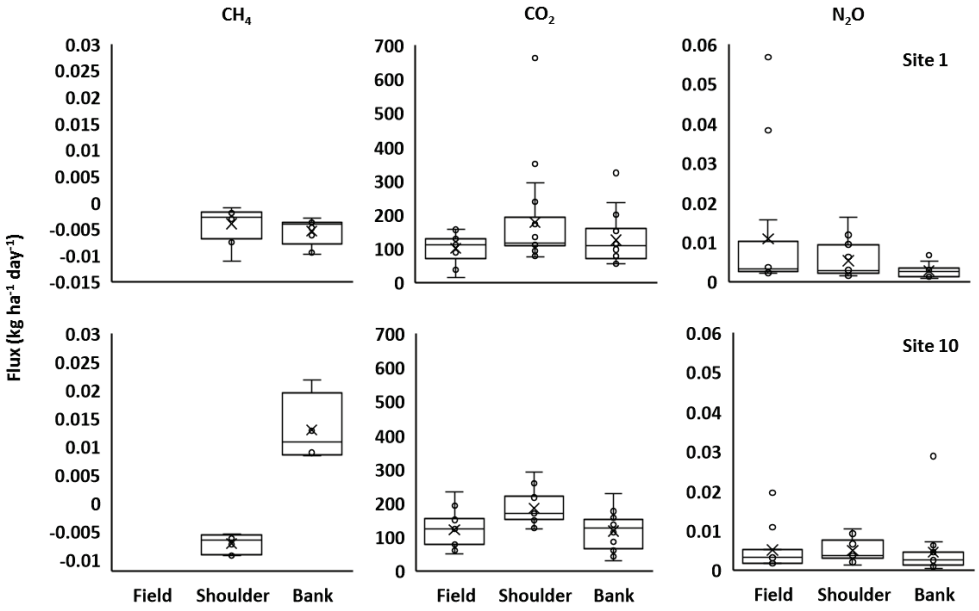

Figure 2-7. Spatial distribution of 2018 surface fluxes from site 1 and 10.

Calculated subsurface fluxes based on measured gas concentration profiles are plotted with the surface fluxes to show a diffusive flux profile with depth (Figure 2-8). The profiles show a general trend of lower fluxes at depth (≥ 40 cm) increasing through the shallow soil horizons (< 40 cm) and generally trending towards the surface flux values. Overall, N_2O and CO_2 subsurface fluxes are positive (diffusing upward) but CH_4 shows both positive and negative fluxes depending on the site and transect location. Methane is diffusing into the shoulder and bank at site 1 as well as the shoulder at site 10 (negative fluxes). However, methane at the site 10 bank is diffusing out of the system. Even though transport direction may vary between CH_4 and the other GHGs, they all produce similar flux magnitudes between 120-40 cm (approximately 10^{-4}-10^{-6} kg ha^{-1} day^{-1}). Above 40 cm, flux magnitudes vary between GHGs with CO_2 producing the largest fluxes. The variability observed between shallow subsurface fluxes is similar to the differences between surface fluxes within each sampling location. The CO_2 shallow

subsurface and surface fluxes vary by $\geq 1.0 \times 10^{2}$ kg ha^{-1} day^{-1} where CH_4 and N_2O generally show $\leq 2.0 \times 10^{-2}$ kg ha^{-1} day^{-1} variation.

These subsurface flux calculations are sensitive to physical parameters, including porosity and moisture content (Eq 2.9; Eq 2.10; Eq 2.11). The porosity values used in this study are similar to values from a nearby Bainsville site that were calculated in 2018 through an associated AGGP study. They found porosity values around 50-60% (I. Widerska, personal communication, March 21, 2018) which agrees with the retention curves used to determine the porosity values in our soil profile. Even though we used qualitative observations to help assign porosity and moisture values to corresponding gas measurements, uncertainties are still prevalent due to heterogeneity in these systems. Altering porosity values by 10% (the range observed by I. Widerska) can change final flux values by a maximum of 32%. Moisture content values decrease flux values logarithmically as they increase from 10% water saturation to 100% water saturation (the range observed in this study). Largest flux decreases are observed when moisture increases from 10% to 40% water saturation as fluxes decrease up to 74% of maximum levels (10% water saturation). Fluxes can decrease another 25% from 40-80% water saturation varying up to 99% of maximum levels. Fluxes show minimal variation when water saturation is $\geq 80\%$ and vary by $< 1\%$ of the maximum flux value as moisture levels reach 100% water saturation. However, our physical characterization of these systems was compared to previous work conducted at the WEBs experimental watershed to ensure we were assigning representative porosity and moisture values where appropriate. This allowed us to create a simplified flux profile that shows a transition

from low fluxes at depth to higher fluxes near surface and agrees with profiles from other studies (M. Maier & Schack-Kirchner, 2014). The positive relationship between the calculated flux profiles and surface fluxes provides confidence in the assumptions made in the subsurface flux calculations.

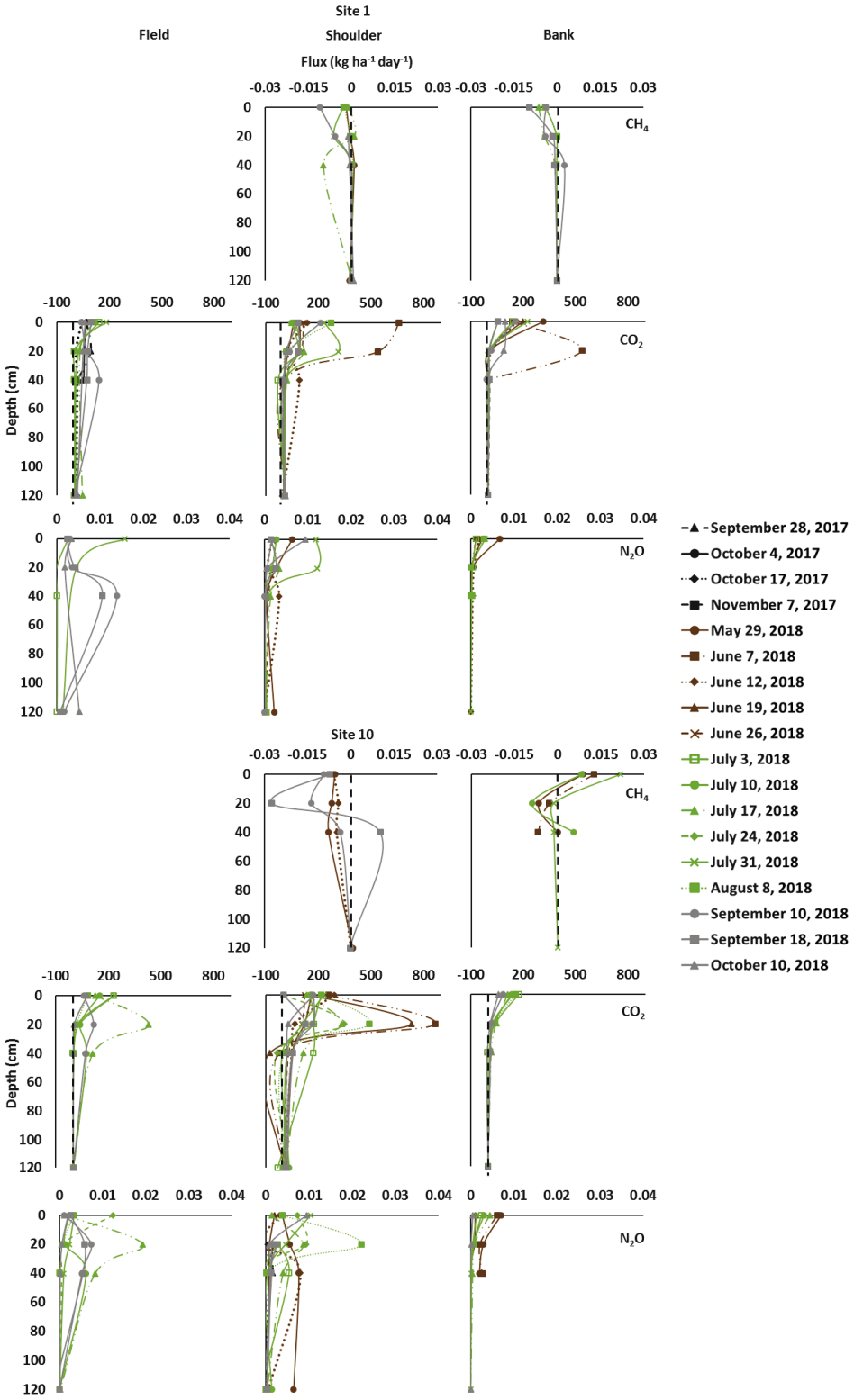

Figure 2-8. Flux profile from sites 1 and 10. Surface fluxes are plotted at 0 cm. Only profiles that include both surface and subsurface flux data are shown in the plots. Nitrous Oxide and methane surface fluxes are the calculated values from the surface flux chamber method where the CO_2 surface fluxes are from the Li-COR results. The dashed black vertical line shows where 0 kg ha^{-1} day^{-1} lies on the plots. CH_4 field plots are excluded from the figure as there aren't any sampling days that contain both subsurface and good regression ($r^2 \geq 0.9$) surface flux data.

Carbon dioxide production rates vary with depth and spatially (Figure 2-9). In the field samples, there is a trend of decreasing production rates between 7.5 cm (64.9 μmol kg^{-1} day^{-1}) and 37.5 cm (17.5 μmol kg^{-1} day^{-1}) before a slight increase to 28.8 μmol kg^{-1} day^{-1} at 75.0 cm. The shoulder samples have a maximum production rate of 85.7 μmol kg^{-1} day^{-1} at 15.0 cm and decrease to a minimum of 28.7 μmol kg^{-1} day^{-1} at 67.5 cm. The upper core samples (7.5-37.5 cm) at the bank have a maximum production rate of 75.6 μmol kg^{-1} day^{-1} at 7.5 cm which decrease to values ≤ 7.9 μmol kg^{-1} day^{-1} at 52.5-75.0 cm

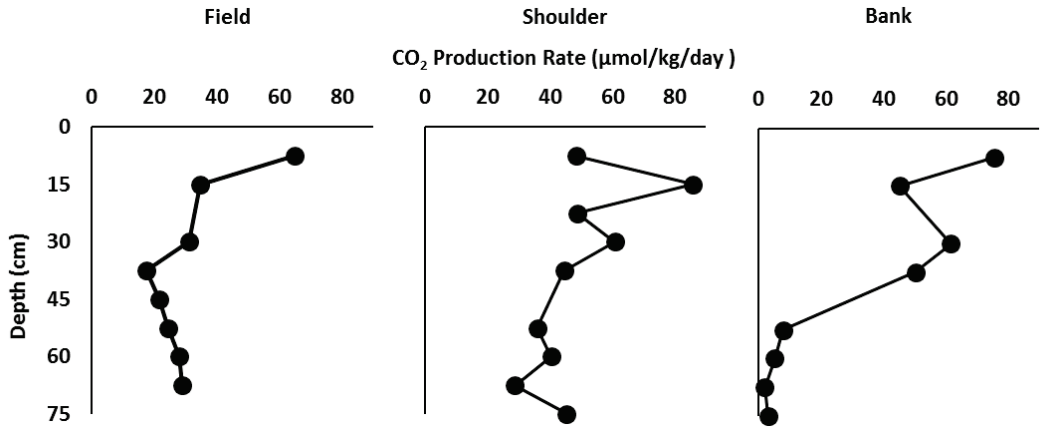

Figure 2-9. CO_2 production rates from the site 1 IsoJar experiment. The cores are 7.5 cm deep and are reported as the lower depth limit (data from Guitard, 2019).

2.4.2 Moisture and Temperature Data

Similar moisture profiles are observed at sites 1 and 10. Generally, lowest volumetric moisture content is observed at shallower depths, increasing to maximums at approximately 45 cm and decreasing somewhat down to 90 cm depth (Figure 2-10). Site 1 field moisture content is lowest at 15 cm with values between 15.1-40.1%. Both shoulders show similar moisture content at 15 cm with values of 9.2-34.6% at site 1 and 5.9-26.8% at site 10. Peak moisture content at site 1 occurs at 45 cm in the field with

values ranging from 39.8-62.8% and at 45-60 cm in the shoulder with values ranging from 26.1-53.1%. Site 10 maximum values range from 22.4-54.0% at 45-60 cm. Moisture content decreases at 90 cm to 30.6-38.1% in the field and 23.8-36.5% in the shoulder at site 1. Moisture content also decreases in the site 10 shoulder at 90 cm with values ranging between 18.5-30.1% except for May 2nd where moisture content remains high at 49.6%. Faulty equipment in the field at site 10 is responsible for the missing field profile.

Temporal variations are evident in the moisture profiles. Highest moisture levels occur at the beginning of May and decrease throughout the agronomic season. Moisture content levels are elevated again in October. There are larger variations in the shoulder profiles than the field, especially at 90 cm where the difference between minimum and maximum values are < 10.0% in the field. Each profile shows less temporal variation at 90 cm when compared to other depths. This region of greater consistency falls within the Cg horizon. The more porous sand and silt horizons are observed at where larger temporal variations are observed. Peak moisture content occurs in the Bg2 horizon.

Subsurface thermocouple data is collected from the shoulders to create a subsurface temperature soil profile of both sites (Figure 2-10). Most temperature profiles show temperature decreasing with depth. Temporal variations are evident as temperatures change by 10-15 ^{o}C throughout the agronomic season. Highest temperatures are observed in the summer (July 3rd-September 6th) at sites 1 and 10 with surface temperatures ranging between 19.6-27.9 ^{o}C and 20.2-30.5 ^{o}C, 10 cm temperatures between 20.3-23.5 ^{o}C and 20.9-25.6 ^{o}C, and 90 cm temperatures between 17-21.5 ^{o}C and 16.8-21.4 ^{o}C,

respectively. Spring (May 2nd-June 26th) and fall (September 10th-October 10th) temperatures are similar to each other but show more variation than the summer profiles. Surface temperatures at sites 1 and 10 range between 10.8-22.9 °C and 11.8-25.9 °C, 10 cm temperatures between 12.5-19.9 °C and 14.4-21.7 °C, and 90 cm temperatures between 10.2-17.8 °C and 8.4-17.7 °C, respectively. Even though seasonal profiles are similar to each other, weekly variation is still observed but reduced to approximately < 5.0 °C within the summer soil profile and < 10.0 °C in the spring and fall soil profile. Larger disparity is found in the surface temperatures, even throughout each season with a < 14.0 °C variations between minimum and maximum values. Subsurface temperatures generally show a moderate but consistent decrease in temperature with depth, where the surface temperatures are usually much larger than the shallowest temperature measurement (5 cm).

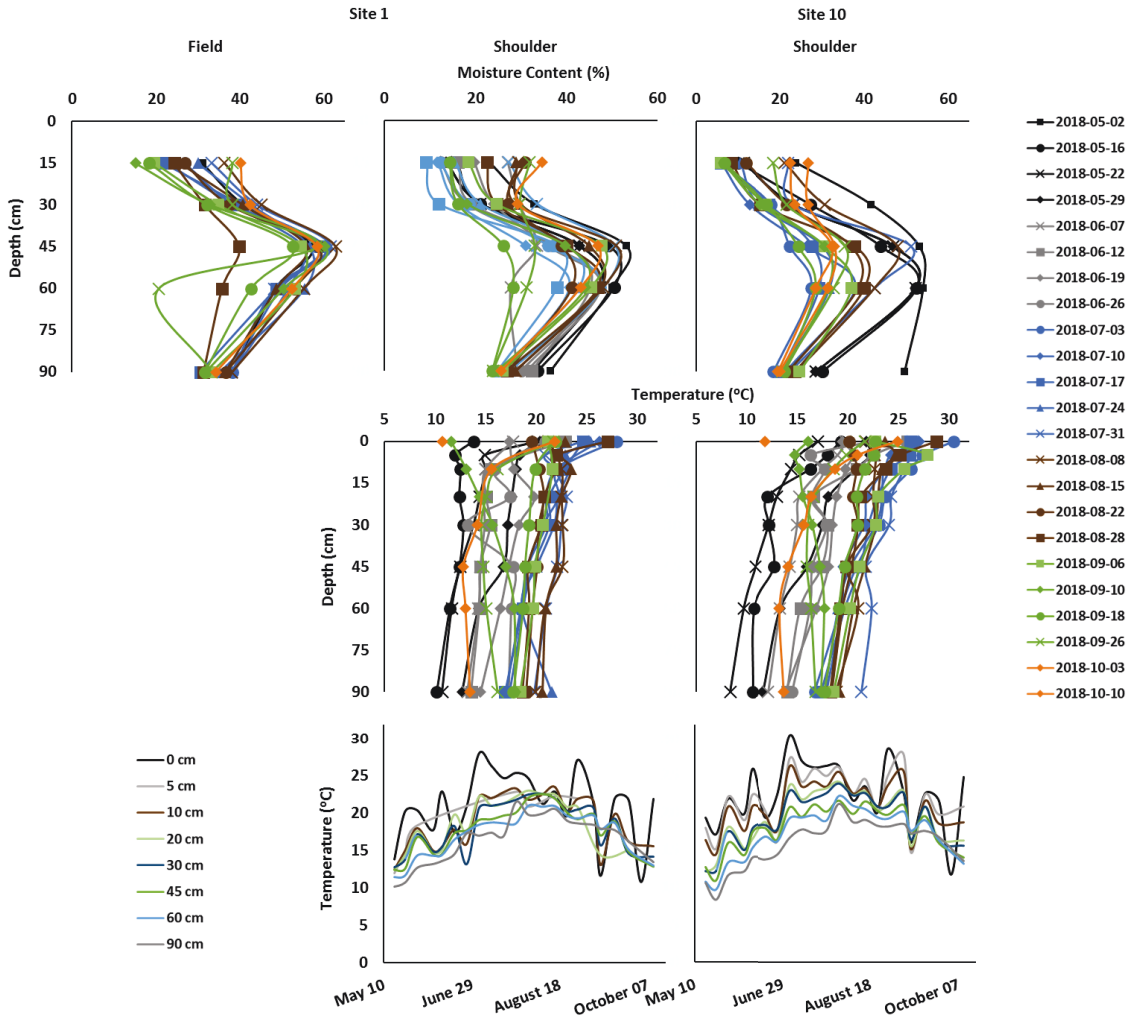

Figure 2-10. 2018 Temperature and moisture profiles from sites 1 and 10.

2.4.3 Geochemical Data

Groundwater and vadose zone results are compiled to show the spatial distribution of pH, ORP, DIC, DOC, NH_3-N and NO_3^- at both sites (Figure 2-11). Due to the limited availability of samples at each depth, no analysis of the depth dependence of these parameters is conducted. A one-way Anova and TukeyHSD test is used to determine the spatial relationship between sampling locations within each site and a Welch two sample t-test is used to show the spatial relationship between corresponding sampling locations between the two sites ($P < 0.05$ is significant).

Most of the samples are neutral with mean pH values of 7.4 (field), 7.8 (shoulder) and 7.1 (bank) at site 1 and 7.4 (field), 7.3 (shoulder) and 7.2 (bank) at site 10. The shoulder at site 1 has higher pH values than the bank ($P = 0.01$), but the shoulder and field as well as the field and bank are similar ($P = 0.25$ and $P = 0.53$). There is no statistical difference between pH values along the site 10 sampling transect ($P = 0.48$). The two sites show no statistical difference between pH values in the field ($P = 0.94$) and the bank ($P = 0.46$); however, the pH in the site 1 shoulder is higher than site 10 ($P = 0.03$). Contrary to pH, ORP shows spatial variation within both sites. At site 1, the bank has reducing ORP values (mean of -33.7 mV) which is lower than the oxidizing values in the shoulder (mean of 212.5 mV; $P = 0.03$) and the field (mean of 159.4 mV; $P = 0.02$). The same relationship is observed at site 10 where reducing ORP values in the bank (mean of -32.6 mV) are lower than the oxidizing values in the shoulder (mean of 169 mV; $P < 0.01$) and the field (mean of 199.1 mV; $P < 0.01$). Corresponding sampling locations at the two sites show no statistical variation in ORP values ($P > 0.05$). It is important to note that the bank samples are predominantly collected from piezometers.

Nitrate at site 1 follows the same trend as ORP with bank NO_3^- values (mean of 0.22 mg L^{-1}) lower than the shoulder (mean of 75.32 mg L^{-1}; $P < 0.01$) and the field (mean of 49.73 mg L^{-1}; $P = 0.03$). At site 10, the shoulder has the highest NO_3^- levels (mean of 64.68 mg L^{-1}) which is statistically higher than the field (mean of 10.66 mg L^{-1}; $P < 0.01$) and the bank (mean of 0.13 mg L^{-1}; $P < 0.01$). Nitrate levels do not vary between the two sites in the field ($P = 0.09$) and shoulder ($P = 0.79$), but site 10 has lower

bank NO_3^- levels than site 1 (P = 0.04). Ammonia levels are comparable throughout the site 1 transect (P = 0.32) with mean values of 0.10 mg L^{-1} in the field and shoulder and 0.54 mg L^{-1} in the bank. Site 10 NH_3-N levels vary throughout the transect with shoulder values (mean of 0.88 mg L^{-1}) being larger than the bank (0.11 mg L^{-1}; P = 0.03). Site 10 field NH_3-N mean levels are 0.2451 mg L^{-1} which are statistically comparable to the shoulder (P = 0.10) and the bank (P = 0.72). Like NO_3^-, NH_3-N levels are the same in the field (P = 0.08) and shoulder (P = 0.79) between the two sites, but lower NH_3-N levels are observed in the bank at site 10 (P = 0.04).

Dissolved inorganic carbon levels are highest in the bank at both sites. At site 1, the bank DIC levels (mean of 114.1 mg L^{-1}) are higher than the shoulder (mean of 38.22 mg L^{-1}; P < 0.01) and the field (mean of 54.19 mg L^{-1}; P < 0.01). The same relationship is observed at site 10 where the field (mean of 59.20 mg L^{-1}) and shoulder (mean of 34.21 mg L^{-1}) are lower than the bank (mean of 87.12 mg L^{-1}; P=0.01 and P<0.01). Sites 1 and 10 only have varying DIC values in the bank (P = 0.0137) where the shoulders and fields are the same (P = 0.71 and P = 0.70). There are no statistical differences between DOC levels throughout the transect at site 1 (P = 0.78) and site 10 (P = 0.27). Site 1 mean DOC values are 18.80 mg L^{-1} (field), 22.14 mg L^{-1} (shoulder) and 23.43 mg L^{-1} (bank) where site 10 values are 20.70 mg L^{-1} (field), 36.18 mg L^{-1} (shoulder) and 36.26 mg L^{-1} (bank). The two sites have the same DOC values in the field (P = 0.61), shoulder (P = 0.31) and bank (P = 0.14).

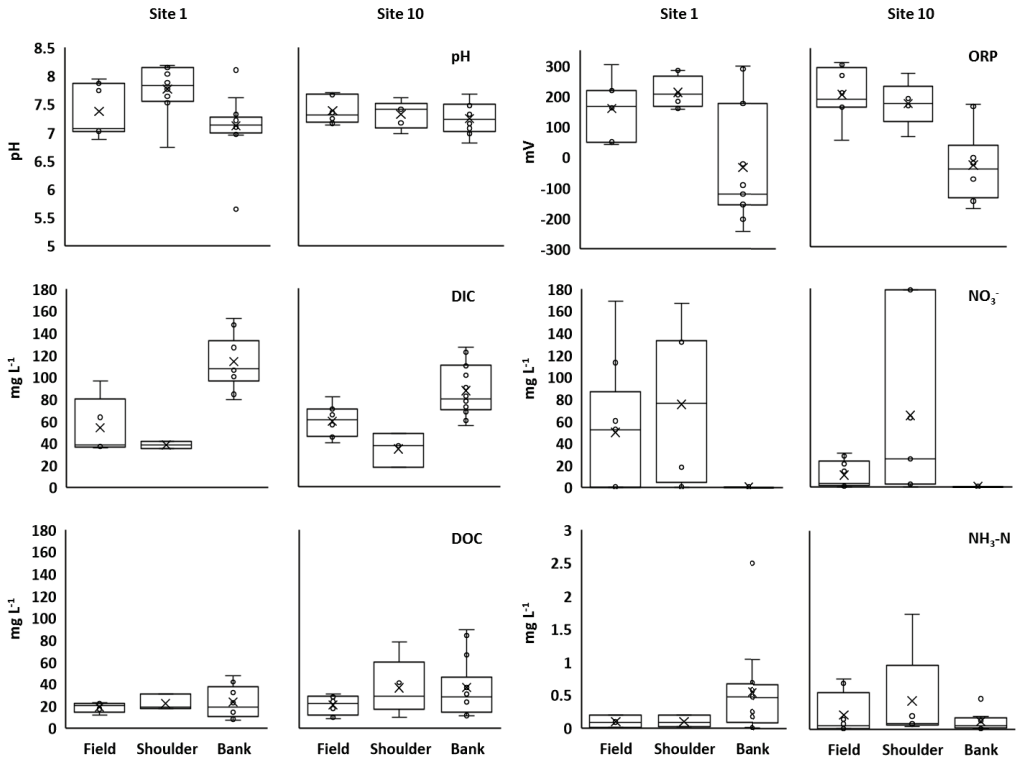

Figure 2-11. Geochemical data collected from piezometers and lysimeters at both sites. Results that were below the analytical detection limit (DL) are reported as ½ the DL (0.13 mg L^{-1} for NO_3^- and 0.01 mg L^{-1} for NH_3-N).

2.4.4 Soil Data

Carbon soil chemistry is shown at two depths (15 cm and 30 cm) and reported as TOC and TIC for both sites (Figure 2-12). Site 1 TOC 15 cm and 30 cm values range between 1.19-1.90% and 1.46-3.23% in the field, 1.80-2.56% and 1.55-2.02% in the shoulder and 1.46-2.20% and 0.06-0.55% in the bank, respectively. Field TOC levels are higher at depth whereas the shoulder has similar TOC values at both depths. Lowest TOC values are observed at 30 cm in the bank with a mean of 0.40%. Similar TIC values are observed at all three sampling locations and range between 0.02-1.18%. Generally, TIC concentrations are lower than TOC levels except in the bank where TIC levels are similar to the 30 cm TOC samples. Site 10 TOC samples show greater depth variation than site 1 as 15 cm and 30 cm samples range between 1.86-2.08% and 1.10-1.44% in the field,

2.58-5.11% and 0.62-2.89% in the shoulder and 1.77-2.35 and 0.47-0.85% in the bank, respectively. Similar to site 1, site 10 TIC values are generally lower than TOC levels and are similar at both depths in the field and bank (0.17-0.69%). Site 10 shows more TIC variation in in the shoulder as 15 cm samples range between 0.03-1.93% and the 30 cm samples range between 0.16-4.15%. Here the deeper soil has higher TIC levels opposed to other sampling locations where TIC levels remain more consistent. There aren't any distinctive temporal trends within site 1; however, site 10 shoulder TOC levels decrease throughout the agronomic season as TIC values increase. Both sites have similar carbon levels, but greater maximum TOC and TIC levels (5.02% and 4.15%) are observed at site 10 on the shoulder.

Nitrogen soil chemistry is also shown at 15 cm and 30 cm and reported as two species; nutrients (NO_3^--N and NO_2^--N) and NH_3-N (Figure 2-12). Nutrient concentrations are mostly larger than NH_3-N levels and highest nutrient levels are observed at shallower depths. At site 1, nutrient levels are similar in the field and shoulder with values ranging from 0.84-2.29 mg L^{-1} at 15 cm and 0.45-1.17 mg L^{-1} at 30 cm. The bank has lower nutrient levels than the other sampling locations with values of 0.47-1.06 mg L^{-1} at 15 cm and 0.05-0.40 mg L^{-1} at 30 cm. Ammonia soil concentrations are similar at both sampling depths in the field and shoulder ranging between 0.02-0.12 mg L^{-1}. The bank has higher NH_3-N levels which range between 0.03-0.43 mg L^{-1} at 15 cm and 0.08-0.22 mg L^{-1} at 30 cm. There aren't distinct temporal trends in the site 1 nitrogen soil chemistry except that there is a slight increase in nutrient concentrations within the shoulder throughout the agronomic season. Site 10 shows greater variation

throughout the sampling transect but nutrient levels are still higher at shallower depths. Nutrient levels are between 0.39-1.50 mg L^{-1} and 0.56-0.93 mg L^{-1} in the field, 0.80-4.14 mg L^{-1} and 0.07-1.95 mg L^{-1} in the shoulder, 0.27-0.65 mg L^{-1} and 0.05-0.08 mg L^{-1} in the bank at 15 cm and 30 cm, respectively. The field NH_3-N values are similar at both depths ranging from 0.033-0.171 mg L^{-1}. Higher NH_3-N values are observed in the shoulder with concentrations of 0.26-4.06 mg L^{-1} at 15 cm and 0.17-1.29 mg L^{-1} at 30 cm. In the bank, 15 cm NH_3-N levels exceed nutrient concentrations and are reported at 0.78-0.99 mg L^{-1}. However, 30 cm NH_3-N concentrations are between 0.18-0.99 mg L^{-1} and are close to bank nutrient values. Similar to the carbon soil data, higher concentrations of nitrogen species are found at site 10 with a maximum NH_3-N concentration of 4.06 mg L^{-1} and nutrient concentration of 4.14 mg L^{-1}. These maximum values are observed in the site 10 shoulder.

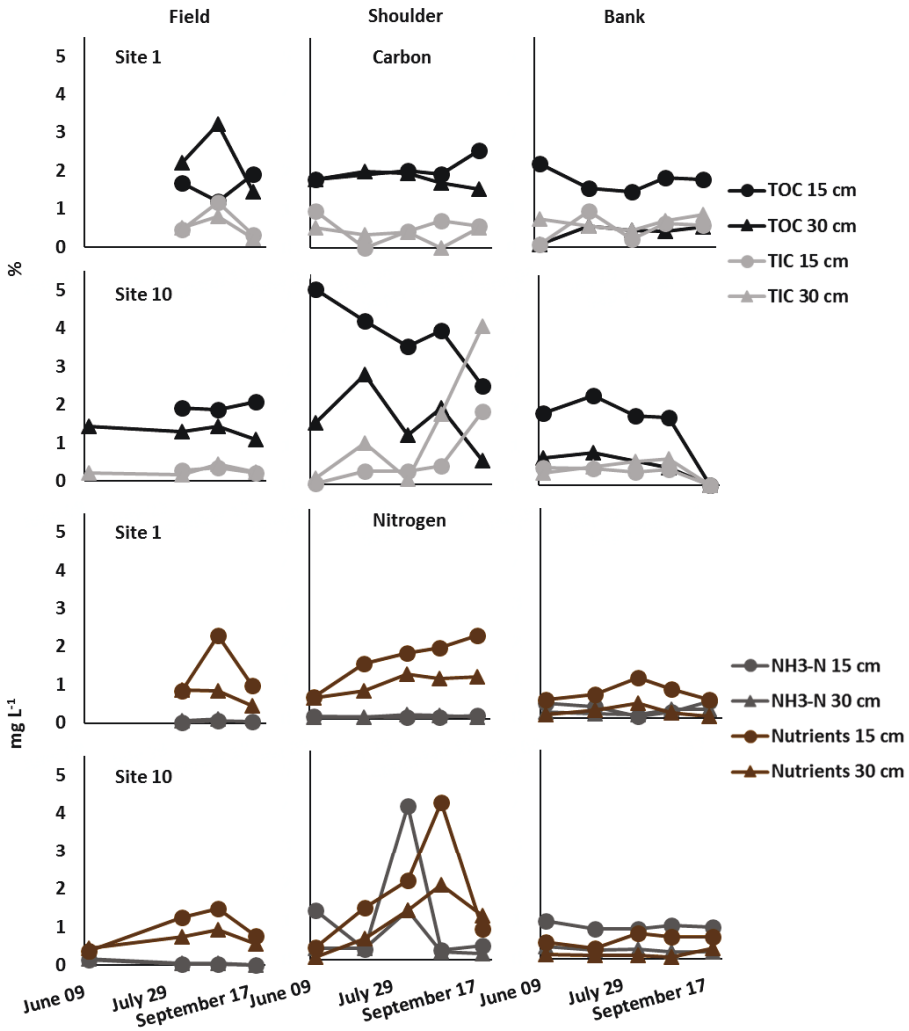

Figure 2-12. Carbon and nitrogen soil sample data from 15 cm and 30 cm at both sites. TIC and TOC values are reported as %C. Nutrients consist of the combined concentrations (mg L^{-1}) of NO_3^--N and NO_2^--N.

Site 1 soil properties vary with depth and show some variation spatially throughout the sampling transect (Table 2-3). In the field, soil characteristics are similar between 15 cm and 40 cm depths. The soil is dominantly silt and clay, 42.8% and 42.8%, respectively at 15 cm. At 40 cm, there is more silt than clay as the soil contains 49.7% and 37.0%, respectively. Both depths contain low amounts of sand with levels of 14.4% at 15 cm and 13.3% at 40 cm. These upper soil samples are rich in organic matter with 3.4% at 15 cm and 4.1% at 40 cm. They have a CEC of 23.5 cmol+ kg^{-1} at 15 cm and 27.6 cmol+ kg^{-1} at

40 cm which is higher than the deeper soil cores. These upper samples are classified as a silty clay at 15 cm and a silty clay loam at 40 cm. There is a noticeable transition at 65 cm as the sample is now classified as a loam. It is dominantly sand (49.3%) and silt (36.9%) but still contains some clay (13.8%). It has much less organic content (0.3%) and lower CEC (7.4 cmol+ kg^{-1}) than the overlying sample. The deepest sample (90 cm) is also noticeably different than the others and is classified as a clay loam. It contains 36.7% sand, 27.4% silt and 35.9% clay. Organic matter levels remain low (0.2%) but the CEC (12.3 cmol+ kg^{-1}) is higher than the 65 cm sample but lower than the shallow samples. The upper shoulder samples (15 cm and 40 cm) are similar to the shallow field samples and are characterized as silty clays. They both contain approximately 19% sand, 40% silt and 25% clay. The 15 cm sample has slightly higher organic matter levels (3.9%) than the 40 cm sample (3.4%), but they both have the same CEC (24.8 cmol+ kg^{-1}). The shoulder 65 cm sample contains more silt (50.7%) than sand (21.2%) and clay (28.1%). This clay loam sample has less organic matter than the overlying samples (2.1%) but contains higher levels than the equivalent depth in the field. It still has a high CEC at 19.0 cmol+ kg^{-1}. The 90 cm sample, a sandy clay loam, is dominantly sand (45.2%) with similar levels of silt (27.8%) and clay (26.9%). Similar to the 90 cm field sample, it also contains low levels of organic matter (0.6%) and a CEC of 12.7. The bank contains different soil characteristics than the other sampling locations along the transect. The 15 cm sample is a loam and contains more sand (40.6%) than the other 15 cm samples. It contains 36.6% silt, 22.9% clay and high levels of organic matter at 3.1%. This loam sample has a slightly lower CEC (17.1 cmol+ kg^{-1}) than other 15 cm samples. The underlying 40 cm sample is characterized as a sandy clay loam as it contains 48.2% sand,

27.2% silt and 24.6% clay. It's organic matter levels of 0.8 and CEC of 9.4 cmol+ kg^{-1} are much lower than the 15 cm sample. The two heavy clay lower samples at 65 cm and 90 cm are similar to each other as they contain 2.8-9.5% sand, 29.1-32.7% silt, 61.5-64.6% clay, 0.6% organic matter and a CEC of 18.4-19.4 cmol+ kg^{-1}.

At site 10, there are similarities between the field and shoulder, but they vary with the profile at the bank (Table 2-3). The field 15 cm and 40 cm samples are similar and contain 12.4-14.1% sand, 29.2-29.8% silt and 29.8-29.2% sand. These silty clay loams have similar CECs (21.7-22.7 cmol+ kg^{-1}) but the 15 cm sample has organic matter levels of 3.7% which is higher than the 2.8% at 40 cm. There is a distinct difference between the silty clay loams and the underlying very fine sandy loam at 65 cm. This sample is predominantly sand (57%) and containing 28.1% silt, 14.9% clay, low levels of organic matter (0.3%) and a CEC of 15.2 cmol+ kg^{-1}. There is another distinct transition at 90 cm as this sample contains less sand (14.3%) but higher levels of silt (41.6%) and clay (44.1%). This silty clay has low organic matter content (0.5%) and a CEC of 14.0 cmol+ kg^{-1}. The 15 cm and 40 cm shoulder samples are similar to the shallow field samples and are also classified as silty clay loams; however, they have much higher organic matter content than any other samples (5.9-6.9%). They contain 15-15.9% sand, 57% silt, 27.1% clay and have a CEC of 27.2-29.4 cmol+ kg^{-1}. The 65 cm sample is similar to the overlying soil as it is a silt loam but has lower organic matter content at 1.3%. Particle size distribution is also similar as it contains 23.1% sand, 56.7% silt and 20.2% clay. It also has a lower CEC which is 15.2 cmol+ kg^{-1}. The 90 cm sample is a very fine sandy loam and is similar to the 65 cm field sample. It has low organic matter content at 0.4%

and a low CEC (8.5 cmol+ kg^{-1}). This sample is mainly sand (64.1%) with some silt (22.4%) and clay (11.7%). The 15 cm bank sample also contains more sand (44.4%) than silt (35.5%) and clay (11.7%). This loam has 3.5% organic matter and a CEC of 17.4 cmol+ kg^{-1}. The 45 cm sample has a similar CEC (17.7 cmol+ kg^{-1}) but lower organic matter content (1%). This sample is characterized as a clay and contains 22.4% sand, 29.3% silt and 48.3% clay. Soil at 65 cm is also dominated by clay (61.7%) but is classified as a heavy clay as it has little sand (5.4%) and moderate levels of silt (32.9%). It still has a similar CEC (19.4 cmol+ kg^{-1}) and organic matter content (0.8%) to the overlying sample. The 90 cm sample still contains very little sand (4.7%) but has more silt (53.7%) than clay (41.6%). This silty clay has less organic matter (0.5%) and a lower CEC (10.2 cmol+ kg^{-1}) than the heavy clay.

Site	Location	Depth	Organic Matter %	Gravel %	Sand %	Silt %	Clay %	CEC (cmol+/kg)	Texture
1	Field	15	3.4	0.0	14.4	42.8	42.8	23.5	Silty clay
1	Field	40	4.1	0.7	13.3	49.7	37.0	27.6	Silty clay loam
1	Field	65	0.3	0.0	49.3	36.9	13.8	7.4	Loam
1	Field	90	0.2	0.2	36.7	27.4	35.9	12.3	Clay loam
1	Shoulder	15	3.9	0.3	19.1	40.0	40.9	24.8	Silty clay
1	Shoulder	40	3.4	0.0	19.0	40.9	40.0	24.8	Silty clay
1	Shoulder	65	2.1	0.0	21.2	50.7	28.1	19.0	Clay loam
1	Shoulder	90	0.6	0.3	45.2	27.8	26.9	12.7	Sandy clay loam
1	Bank	15	3.1	0.3	40.6	36.6	22.9	17.1	Loam
1	Bank	40	0.8	5.4	48.2	27.2	24.6	9.4	Sandy clay loam
1	Bank	65	0.6	0.1	9.5	29.1	61.5	19.4	Heavy clay
1	Bank	90	0.6	0.0	2.8	32.7	64.6	18.4	Heavy clay
10	Field	15	3.7	0.1	12.4	57.8	29.8	22.7	Silty clay loam
10	Field	40	2.8	0.0	14.1	56.6	29.2	21.7	Silty clay loam
10	Field	65	0.3	0.2	57.0	28.1	14.9	8.2	Very fine sandy loam
10	Field	90	0.5	0.4	14.3	41.6	44.1	14.0	Silty clay
10	Shoulder	15	6.9	0.0	15.9	57.0	27.1	27.2	Silty clay loam
10	Shoulder	40	5.9	0.1	15.0	57.0	28.0	29.4	Silty clay loam
10	Shoulder	65	1.3	0.0	23.1	56.7	20.2	15.2	Silt loam
10	Shoulder	90	0.4	0.0	64.1	24.2	11.7	8.5	Very fine sandy loam
10	Bank	15	3.5	0.0	44.4	35.5	20.1	17.4	Loam
10	Bank	40	1.0	0.0	22.4	29.3	48.3	17.7	Clay
10	Bank	65	0.8	0.0	5.4	32.9	61.7	19.4	Heavy clay
10	Bank	90	0.5	0.1	4.7	53.7	41.6	10.2	Silty clay

Table 2-3. Organic matter, particle size distribution, CEC and texture from augered soil cores collected at sites 1 and 10. The cores are reported at the lower depth of the core interval.

2.5 Discussion

2.5.1 Site Characterization

Observed soil properties (Table 2-3) are compared to the Bainsville soil classification (Section 2.2) and qualitative field observations to build site specific soil profiles (Figure 2-13). Similarities in organic matter, CEC and particle size distribution were key factors in determining the depths and lateral extents of subsurface soil horizons. A horizons are typically shallow surface soil layers rich in organic matter (Agriculture and Agri-Food Canada, 1998). Bainsville A horizons are usually 20 cm thick (Table 2-2); however, due to tillage in the top 30 cm of soil in the fields at these sites, the Ap horizon is slightly larger at approximately 30 cm thick. The A horizon is thinner in the shoulder and bank at 20 cm and 15 cm, respectively. Typically, the upper B horizon can resemble similar soil properties to the overlying A horizon but will exhibit a different color due to slight variations in geochemical environment (Agriculture and Agri-Food Canada, 1998). Even though the 0-15 cm and 15-40 cm samples show similar particle size distribution, organic matter content and CEC (Table 2-3), the upper sample is black compared to the 15-40 cm dark brown sample. This is evidence that the two samples contain soils from different horizons. Color variation, plow pan depth and the approximate depth of the known A-B Bainsville horizon interface are used to characterize the A-B interface at these sites. Schut & Wilson (1987) report that the B horizon is mainly sands and silts opposed to the clay dominated C horizon. At these study sites, the B horizon is determined by the deeper core samples that exhibit more sand and silt content than clay. The B horizons are 35 cm thick in the field and 70 cm thick in the shoulder at both sites. The B horizon pinches out before the bank at site 10 but is 25 cm thick in the bank at site

1. The B horizon is subdivided into two sub-horizons (Bg1 and Bg2) based on observed color changes and variable particle size distribution. Bg1 is defined by the upper 20-40 cm of the B horizon. All deeper clay rich core samples are determined to be from the C horizon. The B-C horizon interface occurs at 65 cm in the field and at 90 cm in the shoulder at both sites. The bank C horizon underlies the B horizon at site 1 and appears at 40 cm depth. At site 10, the bank C horizon underlies the A horizon due to the B horizon pinch-out in the upper bank and appears at 15 cm depth.

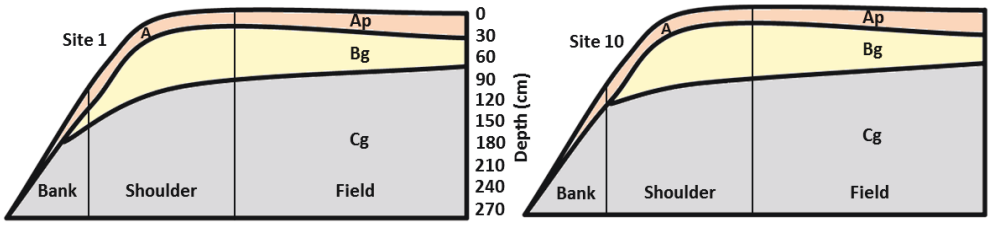

Figure 2-13. Soil profiles for site 1 and 10.

Variations within the soil profiles don't have an influence on the observed temperature profiles. It is evident that temperature decreases at a relatively constant rate with depth (Figure 2-10). This relationship is evidence that the different soil horizons exhibit similar heat transport characteristics. Conduction and convection are two heat transport methods that are usually occurring in soils. Convection is largely influenced by moisture content and advective movement through the system (Koorevaar et al., 1983). Moisture varies throughout the profile with a peak occurring at 45 cm. If convection is the dominant heat transport mechanism, irregularities in the temperature profile should be observed as well. Since temperature decreases linearly with depth, it is apparent that heat transport is likely predominantly conduction and that each horizon displays similar

conductive properties.

Moisture content is related to the soil horizons as there are evident trends within each layer. Shallow measurements have the lowest moisture content which is indicative of higher transpiration, and or evaporation, and or drainage rates than deeper horizons. There is higher TOC content at shallower depths, and it is expected that transpiration increases with TOC content. The A horizon also has a higher hydraulic conductivity than the underlying upper B horizon (Bg1; Table 2-2; Schut & Wilson, 1987) suggesting that it drains better than the lower horizon. Water is likely pooling in this poor drainage region of the B horizon and held near field capacity where there is a thin clay lens observed at approximately 50 cm. The deeper horizons are composed of more sand than the overlying horizons which suggests they should have a lower field capacity. The Bg2 horizon has a higher hydraulic conductivity than Bg1 (Table 2-2), therefor it will drain better than Bg1. This study was conducted during a hot and dry agronomic season. The lack of water availability and the higher field capacity in the Bg1 horizon may be a contributing factor to the lower moisture content at 90 cm.

2.5.2 Gas Production and Consumption

2.5.2.1 CO_2

Higher CO_2 production is expected in oxic soils where there is higher TOC content. High root density and elevated glucose levels are related to higher TOC content which suggests enhanced CO_2 production (Eq 2.1). The IsoJar experiment shows trends of decreasing production with depth which is likely driven by changes in TOC. However, if

soil respiration is the dominant control on CO_2 production in the system, it is possible that the production profile doesn't directly correspond to changes in TOC. Even though root and soil respiration are usually equal in most systems, physical and biologic changes can impact that ratio either increasing or decreasing the overall influence of soil respiration on net CO_2 production (Hanson et al., 2000). If favorable physical conditions for soil respiration such as increased moisture content and temperature (Fierer et al., 2003; Schaufler et al., 2010) are present, it can be the dominant CO_2 producing process. The field and shoulder lower IsoJar cores were taken from sandy horizons with higher water saturation levels than others. Higher moisture levels may cause elevated soil respiration rates despite the limiting presence of organic matter.

2.5.2.2 CH_4

Methane concentrations are highest at the soil/atmosphere interface with concentrations decreasing throughout the soil profile. This trend indicates that the soil is primarily a sink for CH_4. In oxygenated, neutral pH systems, methanotrophs facilitate the oxidation of CH_4 to CO_2 (Topp & Pattey, 2011). The geochemical data shows that these field sites have mean pH values of 7.3-7.8 and are dominantly oxidizing except for the banks. However, the bank geochemical data is mainly from piezometers (≥ 1.5 m deep) and is not necessarily indicative of the shallower soil horizons. Qualitative observations indicate that the upper bank subsurface is usually unsaturated which suggests an oxic environment. Elevated CO_2 production is also indicative that these shallow soils contain higher oxygen levels. Methanotrophy and CO_2 production commonly occur congruently (M. Maier & Schack-Kirchner, 2014) despite CH_4 only having minor contributions to the

overall CO_2 budget. Steep CH_4 downward concentration gradients in the upper 40 cm of soil suggest that methane is being consumed at elevated rates in those shallow zones. Even though methanotrophy is the dominant control of CH_4 in these systems, increased moisture content in the banks can shift the system towards an anaerobic environment and allow methanogenesis to occur. The site 10 bank concentration profile shows a downward concentration gradient which produces an influx in the subsurface at 20 cm; however, the soil surface is emitting CH_4. This is indicative that there is a shallow anaerobic CH_4 producing zone just below the surface causing CH_4 to move both upward and downward. Variability in subsurface redox conditions due to subsurface heterogeneity between the gas rods and surface chamber sampling locations can also cause the discrepancies between the subsurface and surface CH_4 fluxes. Either way, methanogenesis is occurring in areas where CH_4 effluxes are observed.

2.5.2.3 N_2O

High N_2O production is expected to occur in anaerobic regions. Moisture profiles show that there is lower moisture content above 40 cm which indicates that N_2O production is likely occurring at a greater rate in the deeper saturated regions. The concentration profiles show higher concentrations in these deeper, less oxygenated regions. It is important to note that the field is the only sampling region where nitrogen fertilizers are directly applied. The shoulder is near the field, therefor may be exposed to fertilizer due to being in close proximity to application zones. The field and shoulder have higher soil nutrient levels than the bank. Even though the bank is generally more anaerobic than the other sampling locations, due to higher moisture content, it lacks high

levels of nutrients which reduces the amount of N_2O produced. The geochemical data shows low levels of NO_3^- in the reducing environment at the bank which is expected (Ponnamperuma, 1972). However, if the low NO_3^- levels are related to high levels of denitrification, elevated N_2O concentrations are expected which is not observed.

2.5.3 GHG Surface Fluxes

The observed GHG surface fluxes are similar to other studies conducted in this watershed as we observed mean fluxes of 1.4×10^2 kg ha^{-1} day^{-1} for CO_2, 6.1×10^{-2} kg ha^{-1} day^{-1} for N_2O and $< -1.1 \times 10^{-2}$ kg ha^{-1} day^{-1} for CH_4 (Nangia et al., 2013; Van Zandvoort et al., 2017a). Fluxes are reported as effluxes for all CO_2 and N_2O measurements and most CH_4 fluxes. However, reducing conditions can cause some CH_4 effluxes which are observed at the site 10 bank (Smith et al., 2018). There is also spatial variation within the site 10 CO_2 surface fluxes with higher fluxes produced on the shoulder. The site 10 shoulder also has higher shallow TOC content (15 cm depth) which can increase production and generate a greater gradient between 15 cm and the surface, and elevate CO_2 effluxes. Other than that, there are few spatial variations between GHG fluxes even though there are spatial differences between the concentration profiles. This indicates that transport mechanisms control the relationship between gas production and fluxes through the system.

2.5.4 Gas Transport

Carbon dioxide production is highest in the surface soil horizons, but gas measurements show lowest CO_2 concentrations at shallower depths. This relationship

allows us to infer regions of high and low transport as there must be a higher flux where we observe low gas concentrations in a high production zone, or a low flux where high gas concentrations are observed in a low production zone. Subsurface flux calculations show that trend, with larger fluxes occurring in the high production region. This is consistent with Maier & Schack-Kirchner (2014) who show that CO_2 efflux is highest near surface and has an inverse profile to CO_2 concentrations. They suggest that CH_4 consumption occurs in regions where high CO_2 production is observed, therefor higher CH_4 influxes are expected to occur concurrently with higher CO_2 effluxes. This means that the diffusive direction will vary between CH_4 and CO_2 (down and up), but regions of high and low transport should fall within the same sections of the soil profiles. This is apparent in our subsurface flux profile (Figure 2-8) as we observe higher mass fluxes near surface and much lower transport at depth.

Spatial variations in concentration profiles are apparent for both CO_2 and N_2O with maximum concentrations occurring in the fields, yet the fields do not produce highest effluxes. This allows us to infer that there must be a physical or geochemical control on GHG transport. The fields are also the locality where we observe highest water saturation. Moisture content plays a crucial role in gas transport as it can alter soil pore networks, thus lengthening the diffusive pathway by increasing tortuosity. Greenhouse gas diffusivity is much greater through air than water (M. Maier & Schack-Kirchner, 2014; Topp & Pattey, 2011) which indicates that diffusion rates will decrease with water saturation. There is a good correlation between moisture content and fluxes displayed by Spearman's rank-order coefficient (r_s) as higher moisture content corresponds to lower

fluxes (r_s values of -0.47, -0.26 and -0.71 at site 1 and -0.56, -0.40 and -0.72 at site 10 for CO_2, N_2O and CH_4). It is evident that moisture content can alter flux values due to its influence on other the terms (T, S_g) used in subsurface flux calculations (Eq 2.9; Eq 2.10; Eq 2.11).

Concentration gradients are another crucial component of Fick's first law and have a major contribution on diffusive transport. There is a strong statistical relationship between concentration gradients and calculated subsurface fluxes shown by high r_s values for CO_2 and N_2O at site 1 (0.81 and 0.85; insufficient samples to conduct analysis for CH_4) and CO_2, N_2O and CH_4 at site 10 (0.76, 0.71 and 0.64). Higher gradients are observed in shallower soil horizons where they exhibit higher fluxes than deeper horizons. Over time, the lack of transport causes CO_2 and N_2O to accumulate at depth causing a spike in deeper subsurface concentrations. There isn't an increase in CH_4 concentrations in the deeper low flux regions because conditions do not favor CH_4 production, therefor transport is the mechanism causing the observed CH_4 concentrations at depth. It is important to note that moisture is also a significant control on concentration gradients as it has a direct influence on transport pathways as well as an indirect on subsurface concentrations by influencing production rates. These analyses show that gradient is the dominant control on subsurface fluxes; however, they are also strongly impacted directly and indirectly by water saturation levels.

These regression models help illustrate why higher fluxes occur in the upper soil horizons. Visual inspection of the concentration profiles (Figure 2-5) shows that with

many profiles there is a higher gradient near the surface than at depths. There seems to be two distinct gradients, one above 40 cm and one below. These two profiles correspond to regions of high and low fluxes. The lower regions have higher moisture content and lower gradients which together have a major influence in GHG transport. The upper region has a steep gradient and less moisture which allows GHGs to diffusive much faster through this part of the system.

Despite CO_2 and N_2O displaying similar transport trends, there are fundamental differences between the processes driving the concentration profiles. CO_2 is produced at a higher rate in shallower soil horizons due to higher TOC content but is also produced at depth due to favorable moisture conditions. However, the increased moisture content at depth reduces flux magnitudes. Together, high production and high transport near the surface causes the soil to contain low concentrations of CO_2. However, N_2O is produced at depth where anaerobic saturated conditions prevail (Davidson, 1993) but accumulates at these depths due to the lack of transport. Despite shallow horizons exhibiting less favorable production conditions, N_2O is still produced within isolated anaerobic regions (hotspots) throughout the subsurface (Gregorich et al., 2005). Like CO_2, N_2O undergoes higher transport near the surface due to the lack of moisture content, which also increases the concentration gradient in the A and upper B horizons.

Many studies have used either surface or subsurface GHG measurements as proxies for modeling the influence of soil conditions on GHG flux profiles (Hashimoto & Komatsu, 2006; M. Maier & Schack-Kirchner, 2014; Nangia et al., 2013; M. Sunohara et

al., 2016; Van Zandvoort et al., 2017a). Excluding subsurface or surface conditions on developing flux profiles limits the accuracy of the model due to the lack of site-specific data. Our study shows the significance of combining subsurface and surface GHG measurements to accurately build a transport model that relates subsurface flux profiles to measured surface fluxes. Kusa et al. (2008) discuss the importance of using measured surface GHG fluxes to validate assumptions made by the gradient method's flux models. However, the gradient method is limited to calculating subsurface fluxes only between gas sampling depth locations. This excludes the region above the shallowest gas sampling rod and the soil/atmosphere interface which limits the ability to determine transport parameters for that interval (Fujikawa et al., 2007). Our subsurface flux model shows an increasing transport trend from deep to shallow soil horizons reaching a maximum flux at the surface. Even though there is a gap in the subsurface data set, the smooth transition between low fluxes at depth and high fluxes at the surface validates the assumptions made within the subsurface flux model and shows the importance of using real data to build such models.

Even though subsurface and surface GHG measurements were coupled to depict GHG transport behavior within this system, errors are still prevalent. In general, our flux model shows a trend of increasing to decreasing GHG flux with depth, however, some profiles show higher fluxes in the shallow subsurface than the soil/atmosphere boundary. There is spatial disparity between GHG surface chambers subsurface sampling equipment, therefor heterogeneity in the system may cause irregularities within the data set. Also, It is possible that slight variations in barometric pressure can cause air to

oscillate within shallow soil pores (Maier et al., 2012). This can add an advective component to the system causing anomalies in the flux profiles.

Although there are minimal spatial differences in surface GHG fluxes throughout the sampling transects, scaling each locations' mean GHG emissions to the true footprint of each location shows that there are significant differences between the field, shoulder and bank. A standard tile drained site at WEBs is 500 m long and 100 m wide and consists of one riparian zone with a 1 m wide shoulder and 3 m wide bank. A typical site has an approximate field footprint of 5 ha, shoulder footprint of 0.01 ha and a bank footprint of 0.03 ha. A field emits on average 5.5×10^{2} kg day^{-1} of CO_2 and 4.0×10^{-2} kg day^{-1} of N_2O (insufficient CH_4 data points to calculate an accurate value). A shoulder emits an average of -6.5×10^{-5} kg day^{-1} of CH_4, 1.9 kg day^{-1} of CO_2 and 5.0×10^{-5} kg day^{-1} of N_2O. A bank emits an average of 1.1×10^{-4} kg day^{-1} of CH_4, 3.8 kg day^{-1} of CO_2 and 1.1×10^{-4} kg day^{-1} of N_2O. There is a direct relationship between the sampling locations footprint and the magnitude of their overall emissions based on surface area; however, CH_4 fluxes vary from influxes on the shoulder to effluxes on the bank, showing that spatial changes have a greater influence on net emissions than the surface area of the locations.

Temporal trends are evident in all subsurface data (GHG concentrations, GHG fluxes, temperature and moisture) but only temperature shows seasonal trends with higher temperatures in the summer than the other seasons. Despite the temporal variations in the data set, they do not correspond to GHG surface fluxes. Only CO_2 shows a slight trend of

decreasing fluxes throughout the agronomic season where the other GHGs show weekly variation like the subsurface data set. Despite there being evident temporal changes within the data, our weekly sampling regime is unable to explain such variations.

2.6 Conclusion

Sites 1 and 10 exhibit similar soil and GHG concentration profiles despite having different riparian zone vegetation cover. Both sites show spatial variation within the CO_2 and N_2O concentration profiles along each sampling transect yet they show minimal spatial variation in surface flux emissions. However, CH_4 emissions vary spatially along the sampling transects as redox conditions change. Methane effluxes are observed in the bank at site 10 opposed to the influxes at all other sampling locations. In general, there appears to be significant spatial variations in subsurface GHG concentrations that are not reflected in surface fluxes. There are disparities in weekly subsurface gas concentrations yet there are no distinct temporal trends as subsurface gas concentrations are constantly changing on a weekly basis. However, surface CO_2 fluxes show a temporal trend of decreasing emissions throughout the agronomic season. Since highest subsurface gas concentrations do not produce highest surface fluxes, gas transport processes are responsible for relating subsurface GHG concentrations to surface fluxes.

Diffusion appears to be the dominant transport mechanism observed within these systems. Higher gas concentrations are observed at depth when effluxes are observed and at the surface when influxes occur. Concentration gradients are the driving force behind subsurface transport, but moisture content is also an important control. Water saturation levels have a direct impact on GHG production rates and physical transport paths. The upper soil horizons (A and Bg1) have a greater influence on surface GHG fluxes due to higher concentration gradients and lower moisture content. Spatial variations observed within the GHG concentration profiles indicates that production rates may vary spatially,

but the lack in spatial disparity in surface emissions shows that overall high concentrations don't cause higher effluxes.

CO_2 is produced at greater rates in shallow soil horizons (A and Bg1) where there is increased TOC and organic matter, favorable conditions for root/soil respiration. However, increased transport reduces the subsurface concentrations measured in those zones. Greater N_2O production occurs in deeper soil horizons (Bg2 and Cg) but unlike the high production zone for CO_2, increased moisture limits gas mobility causing N_2O to accumulate at those depths. There are also pockets of elevated N_2O production within the shallow horizons due to small anaerobic regions. These shallow high production zones undergo elevated transport like CO_2 and result in lower N_2O concentrations than the deeper soil horizons. In these systems, methane predominately undergoes methanotrophy except where reducing subsurface conditions allow methanogenesis to dominate (Site 10 bank). Atmospheric CH_4 levels diffuse downward through oxidizing soil horizons, undergoing greater transport near the surface that at depth. Reducing soils produce CH_4 causing it to diffuse upward throughout the system. Each GHG shows a trend of increased transport in the less saturated A and upper Bg1 soil horizons than the higher saturated underlying lower Bg1, Bg2 and Cg horizons.

This study shows that the gradient method is a suitable way of understanding how GHGs are behaving within the subsurface and are useful in building a subsurface flux model. It is important to couple gradient measurements with surface flux data to ensure the diffusive model is correct and reasonable assumptions are made. This studies'

subsurface diffusive model shows the relationship between physical soil parameters, subsurface GHG concentrations and surface GHG emissions. This understanding will help future studies determine how land use change may influence subsurface and surface GHG behavior within these systems. It can also help develop more detailed transport models to further our understanding of the relationships specified above.

2.7 References

Agriculture and Agri-Food Canada. (2013). South Nation Watershed -Map. Retrieved from http://www.agr.gc.ca/eng/?id=1298408944986

Ambus, P., & Christensen, S. (1994). Measurement of N_2O emission from a fertilized grassland: An analysis of spatial variability. *Journal of Geophysical Research*, *99*(D8), 16549–16555. https://doi.org/10.1029/94jd00267

Ball, B. C. (2013). Soil structure and greenhouse gas emissions: A synthesis of 20 years of experimentation. *European Journal of Soil Science*, *64*(3), 357–373. https://doi.org/10.1111/ejss.12013

Ball, Bruce C., Scott, A., & Parker, J. P. (1999). Field N_2O, CO_2 and CH_4 fluxes in relation to tillage, compaction and soil quality in Scotland. *Soil and Tillage Research*, *53*(1), 29–39. https://doi.org/10.1016/S0167-1987(99)00074-4

Canada, A. and A.-F. (1998). *The Canadian System of Soil Classification*. Retrieved from http://sis.agr.gc.ca/cansis/taxa/cssc3/chpt02_a.html#soilhorizons

Cole, C., Duxbury, J., & Freney, J. (1997). Global estimates of potential mitigation of greenhouse gas emissions by agriculture. *Nutrient Cycling in Agroecosystems*, *49*(1–3), 221–228. https://doi.org/10.1023/A:1009731711346

Crabbé, P., Lapen, D. R., Clark, H., Sunohara, M., & Liu, Y. (2012). Economic benefits of controlled tile drainage: Watershed Evaluation of Beneficial Management Practices, South Nation River basin, Ontario. *Water Quality Research Journal*, *47*(1), 30–41. https://doi.org/https://doi.org/10.2166/wqrjc.2012.007

Davidson, E. (1993). *Soil Water Content and the Ratio of Nitrous Oxide to Nitric Oxide Emitted from soil*. https://doi.org/10.1007/978-1-4615-2812-8_20.

Davidson, E. A., Keller, M., Erickson, H., Verchot, L. V, & Veldkamp, E. (2000). Testing a Conceptual Model of Soil Emissions of Nitrous and Nitric Oxides. *BioScience*, *50*(8), 667–680. https://doi.org/10.1641/0006-3568(2000)050[0667:tacmos]2.0.co;2

Doucet, A.-M. (2019). *Comparing Greenhouse Gas Fluxes from Distinct Microecosystems in Agricultural Drainage Networks*. University of Ottawa.

Dutaur, L., & Verchot, L. V. (2007). A global inventory of the soil CH_4 sink. *Global Biogeochemical Cycles*, *21*(4), n/a-n/a. https://doi.org/10.1029/2006GB002734

Duxbury, J. M. (1994). The significance of agricultural sources of greenhouse gases. *Fertilizer Research*, *38*(2), 151–163. https://doi.org/10.1007/BF00748775

Earth, G. (2019). No Title.

ECCC. (2018). *National Inventory Report 1990–2016: Greenhouse Gas Sources and Sinks in Canada*. Retrieved from https://www.canada.ca/en/environment-climate-

Evans, B. R. O., Skaggs, R. W., & Giiliam, J. W. (1995). CONTROLLED VERSUS CONVENTIONAL DRAINAGE EFFECTS ON WATER QUALITY By Robert O. Evans,· Member, ASCE, R. Wayne Skaggs,2 and. *Irrigation and Drainage Engineering*, *121*(4), 271–276.

Fierer, N., Allen, A. S., Schimel, J. P., & Holden, P. A. (2003). Controls on microbial CO_2 production: A comparison of surface and subsurface soil horizons. *Global Change Biology*, *9*(9), 1322–1332. https://doi.org/10.1046/j.1365-2486.2003.00663.x

Fujikawa, T., Takamatsu, R., Nakamura, M., & Miyazaki, T. (2007). Estimation of

temporal change and spatial variability in CO_2 efflux from the soil surface of agricultural fields. *Jpn. J. Soil. Sci. Plant Nutr*, 487–495.
Gilliam, J. W., Skaggs, R. W., & Weed, S. B. (1979). Drainage Control to Diminish Nitrate Loss from Agricultural Fields1. *Journal of Environmental Quality*, *8*(1), 137. https://doi.org/10.2134/jeq1979.00472425000800010030x
Government of Canada. (2013). Description of soil ONBIVSS~~~A (BAINSVILLE). Retrieved from http://sis.agr.gc.ca/cansis/soils/on/BIV/SS~~~/A/description.html
Gregorich, E. G., Rochette, P., VandenBygaart, A. J., & Angers, D. A. (2005). Greenhouse gas contributions of agricultural soils and potential mitigation practices in Eastern Canada. *Soil and Tillage Research*, *83*(1 SPEC. ISS.), 53–72. https://doi.org/10.1016/j.still.2005.02.009
Guitard, E. (2019). *Tracing CO_2 Emissions from Agricultural Soil Respiration with Bomb Pulse ^{14}C*. University of Ottawa.
Gunter, W. D., Wong, S., Cheel, D. B., & Sjostrom, G. (1998). Large CO_2 Sinks : Their role in the mitigation of greenhouse gases from an international, national (Canadian) and provincial (Alberta) perspective, *61*, 209–227.
HACH. (2015). Nitrogen, Ammonia, Salicylate Method, 0.02- 2.5 mg/L LR.
HACH. (2017). Phosphorus, Reactive (Orthophosphate). https://doi.org/DOC316.53.01119
HACH. (2018). Phenolphthalein and Total Alkalinity 10 to 4000 mg/L as $CaCO_3$.
Hanson, P. J., Edwards, N. T., Garten, C. T., & Andrews, J. A. (2000). Separating root and soil microbial contributions to soil respiration: respiration: A review ofmethods and observations, (C), 115–146. https://doi.org/10.1023/A:1006244819642
Hashimoto, S., & Komatsu, H. (2006). Relationships between soil CO_2 concentration and CO_2 production, temperature, water content, and gas diffusivity: Implications for field studies through sensitivity analyses. *Journal of Forest Research*, *11*(1), 41–50. https://doi.org/10.1007/s10310-005-0185-4
Hefting, M. M., Bobbink, R., & Caluwe, H. De. (2003). Nitrous Oxide Emission and Denitrification in Chronically Nitrate-Loaded Riparian Buffer Zones, 1194–1203.
Koorevaar, P., Menelik, G., & Dirksen, C. (1983). Heat Transport in Soil. In *Elements of Soil Physics* (pp. 193–204). Amsterdam: Elesvier Science B.V.
Kusa, K., Sawamoto, T., Hu, R., & Hatano, R. (2008). Comparison of the closed-chamber and gas concentration gradient methods for measurement of CO_2 and N_2O fluxes in two upland field soils. *Soil Science and Plant Nutrition*, *54*(5), 777–785. https://doi.org/10.1111/j.1747-0765.2008.00292.x
Maier, M., & Schack-Kirchner, H. (2014). Using the gradient method to determine soil gas flux: A review. *Agricultural and Forest Meteorology*, *192–193*, 78–95. https://doi.org/10.1016/j.agrformet.2014.03.006
Maier, Martin, Schack-Kirchner, H., Aubinet, M., Goffin, S., Longdoz, B., & Parent, F. (2012). Turbulence Effect on Gas Transport in Three Contrasting Forest Soils. *Soil Science Society of America Journal*, *76*(5), 1518. https://doi.org/10.2136/sssaj2011.0376
Mayer, K. U., Frind, E. O., & Blowes, D. W. (2002). Multicomponent reactive transport modeling in variably saturated porous media using a generalized formulation for kinetically controlled reactions. *Water Resources Research*, *38*(9), 13-1-13–21. https://doi.org/10.1029/2001wr000862

Mielnick, P. C., & Dugas, W. A. (2000). Soil CO_2 flux in a tallgrass prairie, *32*, 221–228.
Millington, R. J. (1959). Gas Diffusion in Porous Media. *Science*, *130*, 100–102.
Moncrieff, J. B., & Fang, C. (1999). A model for soil CO_2 production and transport 1: Model development. *Agricultural and Forest Meteorology*, *95*(4), 225–236.
Nangia, V., Sunohara, M. D., Topp, E., Gregorich, E. G., Drury, C. F., Gottschall, N., & Lapen, D. R. (2013). Measuring and modeling the effects of drainage water management on soil greenhouse gas fluxes from corn and soybean fields. *Journal of Environmental Management*, *129*, 652–664. https://doi.org/10.1016/j.jenvman.2013.05.040
Ng, H. Y. F., Tan, C. S., Drury, C. F., & Gaynor, J. D. (2002). Controlled drainage and subirrigation influences tile nitrate loss and corn yields in a sandy loam soil in Southwestern Ontario. *Agriculture, Ecosystems and Environment*, *90*(1), 81–88. https://doi.org/10.1016/S0167-8809(01)00172-4
Oertel, C., Matschullat, J., Zurba, K., Zimmermann, F., & Erasmi, S. (2016). Greenhouse gas emissions from soils—A review. *Chemie Der Erde - Geochemistry*, *76*(3), 327–352. https://doi.org/10.1016/j.chemer.2016.04.002
Pihlatie, M., Syväsalo, E., Simojoki, A., Esala, M., & Regina, K. (2004). Contribution of nitrification and denitrification to N_2O production in peat,clay and loamy sand soils under different soil moisture conditions, 135–141.
Ponnamperuma, F. N. (1972). The chemistry of submerged soils. *Advance in Agronomy*, *24*, 29–96.
Prather, M., Derwent, R., Ehhalt, D., Fraser, P., Sanhueza, E., & Zhou, X. (1995). *Other trace gases and atmospheric chemistry*. *Climate Change 1994: Radiative Forcing of Climate Change and an Evaluation of the IPCC IS92 Emission Scenarios*. https://doi.org/10.1007/978-3-642-79287-8_1
Qi, H., & Altinakar, M. S. (2011). Vegetation Buffer Strips Design Using an Optimization Approach for Non-Point Source Pollutant Control of an Agricultural Watershed, 565–578. https://doi.org/10.1007/s11269-010-9714-9
Reay, D. S., Davidson, E. A., Smith, K. A., Smith, P., Melillo, J. M., Dentener, F., & Crutzen, P. J. (2012). Global agriculture and nitrous oxide emissions. *Nature Climate Change*, *2*(6), 410–416. https://doi.org/10.1038/nclimate1458
Rochette, P., & Bertrand, B. (2008). *Soil Surface Gas Emissions*. (M. R. Carter & E. G. Gregorich, Eds.), *Soil Sampling and Methods of Analysis*. https://doi.org/10.1201/9781420005271.ch18
Rochette, P., & Hutchinson, G. L. (2005). Measurement of Soil Respiration in situ: Chamber Techniques. Retrieved from http://digitalcommons.unl.edu/usdaarsfacpub%0Ahttp://digitalcommons.unl.edu/usdaarsfacpub/1379
Rumble, J. R. (2018). *CRC Handbook of Chemistry and Physics*. (F. CRC Press/Taylor & Francis, Boca Raton, Ed.) (99th ed.). Boca Raton. Retrieved from http://hbcponline.com/faces/documents/06_40/06_40_0001.xhtml?search=true
Russow, R., Sich, I., & Neue, H.-U. (2000). The formation of the trace gases NO and N_2O in soils by the coupled processes of nitrification and denitrification: Results of kinetic ^{15}N tracer investigations. *Chemosphere - Global Change Science*, *2*, 359–366. https://doi.org/10.1016/S1465-9972(00)00012-X
Schaufler, G., Kitzler, B., Schindlbacher, A., Skiba, U., Sutton, M. A., & Zechmeister-

Boltenstern, S. (2010). Greenhouse gas emissions from European soils under different land use: Effects of soil moisture and temperature. *European Journal of Soil Science*, *61*(5), 683–696. https://doi.org/10.1111/j.1365-2389.2010.01277.x

Schut, L. W., & Wilson, E. A. (1987). *The soils of the regional municipality of Ottawa-Carleton*. *Ontario Institute of Pedology* (Vol. 2).

Smith, K. A., Ball, T., Conen, F., Dobbie, K. E., Massheder, J., & Rey, A. (2018). Exchange of greenhouse gases between soil and atmosphere: interactions of soil physical factors and biological processes. *European Journal of Soil Science*, *69*(1), 10–20. https://doi.org/10.1111/ejss.12539

South Nation Conservation. (2017). *Vegetation Survey of Twelve Sites within the Watershed Evaluation of Beneficial Management Practices Experimental Watersheds*.

Stumm, W., & Morgan, J. J. (2012). *Aquatic Chemistry: chemical equilibria and rates in natural waters* (3rd ed.). New York: John Wiley & Sons.

Sunohara, M., Gottschall, N., Craiovan, E., Wilkes, G., Topp, E., Frey, S. K., & Lapen, D. R. (2016). Controlling tile drainage during the growing season in Eastern Canada to reduce nitrogen, phosphorus, and bacteria loading to surface water. *Agricultural Water Management*, *178*(3), 159–170. https://doi.org/10.1016/j.agwat.2016.08.030

Sunohara, M. D., Craiovan, E., Topp, E., Gottschall, N., Drury, C. F., & Lapen, D. R. (2014). Comprehensive Nitrogen Budgets for Controlled Tile Drainage Fields in Eastern Ontario, Canada. *Journal of Environment Quality*, *43*(2), 617. https://doi.org/10.2134/jeq2013.04.0117

Sunohara, M. D., Gottschall, N., Wilkes, G., Craiovan, E., Topp, E., Que, Z., et al. (2015). Long-Term Observations of Nitrogen and Phosphorus Export in Paired-Agricultural Watersheds under Controlled and Conventional Tile Drainage. *Journal of Environment Quality*, *44*(5), 1589. https://doi.org/10.2134/jeq2015.01.0008

Topp, E., & Pattey, E. (2011). Soils as sources and sinks for atmospheric methane. *Canadian Journal of Soil Science*, *77*(2), 167–177. https://doi.org/10.4141/s96-107

Tubiello, F. N., Salvatore, M., Ferrara, A. F., Golec, C., Jacobs, H., Flammini, A., et al. (2015). The Contribution of Agriculture , Forestry and other Land Use activities to Global Warming , 1990 – 2012, 2655–2660. https://doi.org/10.1111/gcb.12865

Whiting, G. J., & Chanton, J. P. (1993). Primary production control of methane emission from wetlands, *364*(August), 794–795.

Whiting, Gary J, & Chanton, J. P. (2001). Greenhouse carbon balance of wetlands : methane emission versus carbon sequestration, 521–528.

Wicklund, R. E., & Richards, N. R. (1962a). Soil Map of Russell County Ontario. *Ontario Soil Survey*, (33).

Wicklund, R. E., & Richards, N. R. (1962b). Soil Survey of Russell and Prescott Counties. *Ontario Soil Survey*, (33).

World Bank Group (2019). Agriculture methane emissions (% of total). Retrieved from https://data.worldbank.org/indicator/en.atm.meth.ag.zs

Van Zandvoort, A., Lapen, D. R., Clark, I. D., Flemming, C., Craiovan, E., Sunohara, M. D., et al. (2017). Soil CO_2, CH_4, and N_2O fluxes over and between tile drains on corn, soybean, and forage fields under tile drainage management. *Nutrient Cycling in Agroecosystems*, *109*(2), 115–132. https://doi.org/10.1007/s10705-017-9868-4

Van Zandvoort, A., Clark, I. D., Flemming, C., Craiovan, E., Sunohara, M. D.,

Gottschall, N., et al. (2017). Using 13C isotopic analysis to assess soil carbon pools associated with tile drainage management during drier and wetter growing seasons. *Agricultural Water Management*, *192*, 232–243. https://doi.org/10.1016/j.agwat.2017.06.012

3.0 Using ^{14}C as an Indicator for CO_2 Transport Within Tile Drained Agriculture Systems

3.1 Introduction

The agriculture industry plays a major role in carbon cycling and have been linked to current climate issues. Agriculture contributes 8.5% of Canada's total GHG emissions with enteric fermentation and agriculture soils being the two major contributors (ECCC, 2018). In 2016, CO_2 was responsible for 79% of Canada's GHG emissions. Overall, there has been a 3.8% decrease in total Canadian emissions between 2005 and 2016, yet there have been minimal changes in agriculture output during that time (ECCC, 2018).

Land use changes can modify the carbon budget by altering the source and sink capacity of the subsurface (Lal, 2004). The biosphere is an important CO_2 sink as it is sensitive to environmental changes that can influence the balance between production and sequestration of CO_2 (Gunter et al., 1998b). Major terrestrial carbon pools are found in forests, grasslands and wetlands and are linked to two main carbon sources; CO_2 and vegetation (Janzen, 2004). These pools are responsible for sequestering approximately 17% of atmospheric CO_2; however, 1500 Gt of labile carbon is present in soils which can contribute to significant carbon losses from root and soil respiration (Clark, 2015).

Root and soil respiration are the two main processes responsible for CO_2 production in agriculture soils (Oertel et al., 2016; Stumm & Morgan, 2012);

$$C_6H_{12}O_6 + 6O_2 \rightarrow 6CO_2 + 6H_2O \qquad (3.1)$$

Plants uptake atmospheric CO_2 via photosynthesis (opposite reaction as Eq 3.1) producing organic carbon compounds which are consumed by microbes to facilitate soil respiration or root respiration (Janzen, 2004).

There are noticeable carbon losses (33% of the organic carbon stock) from soils in cultivated areas due to the disruption of these shallow sequestered carbon pools (Cole et al., 1997). Agriculture activity can enhance carbon mineralization thus increasing soil CO_2 outputs (Gregorich et al., 1998, 2005; Lal, 2004). Tilled soils are constantly reworked which mobilizes organic carbon and distributes it evenly within the tilled layer (Alvarez et al., 1995). This uniform distribution of organic matter increases the accessibility of microbial respiration sites. Even though surface soil horizons are known to contain high concentrations of organic carbon, the deeper layers are much thicker and can also contain high levels of organic carbon (Fierer et al., 2003). It is important to quantify CO_2 production in these upper and lower horizons to identify their contributions to the overall carbon budget.

Subsurface measurements are used to monitor in situ subsurface CO_2 concentrations in soils. Higher CO_2 concentrations are found at depth and can reach concentrations upwards of 40000 ppm (Chapter 2; Hashimoto & Komatsu, 2006). These elevated subsurface concentrations are usually the result of low transport, not high production rates as elevated concentrations plot inversely to flux profiles (M. Maier & Schack-Kirchner, 2014). High and low degrees of water saturation can hinder production rates thus altering subsurface CO_2 concentration gradients which influences fluxes (Moncrieff & Fang, 1999). Elevated CO_2 production is expected in soil horizons with approximately 40% water saturation (Schaufler et al., 2010).

Radioisotopes are created by the cosmogenic rays altering the atomic structure of

existing atoms (Kovaltsov et al., 2012). Decay rates are used to define the age of radioisotopes (Clark, 2015);

$$n_t = n_o e^{-\lambda t} \quad (3.2)$$

$$\ln 2 = \lambda T_{1/2} \quad (3.3)$$

The decay constant (λ) is related to the half-life ($T_{1/2}$) of the specific radioisotope which is used to determine the time (t) required to create the current ratio of radioisotopes to stable isotopes (n_t) versus the initial pre-decay isotopic ratio (n_o). Radiocarbon (^{14}C), is a radioisotope useful for dating carbon pools within the carbon cycle as it is unstable and decays with time (Sheridan, 1990). Radiocarbon has a half-life of 5730 years (Clark, 2015) but is constantly being formed in the upper atmosphere where it eventually becomes part of CO_2 molecules and incorporated in the carbon cycle (Bolin et al., 1979; Sheridan, 1990). Organisms will exhibit the atmospheric ^{14}C signatures of their lifetime. Once dead, they stop uptaking carbon and their ^{14}C signatures will change based on the ^{14}C decay rate making them useful dating tools. Radiocarbon signatures are commonly reported as $D^{14}C$ which exhibits a per mil enrichment or depletion relative to a known standard (Stenström et al., 2011; Stuiver & Polach, 1977). This term is age corrected and accounts for isotope fractionation. Fraction modern carbon ($F^{14}C$) is used to report modern ^{14}C values (younger than 1950) and is calculated using the samples $^{14}C/^{12}C$ value versus a standard 1950 $^{14}C/^{12}C$ value (Crann et al., 2017; Reimer et al., 2004).

Nuclear bomb tests in the 1950's and early 1960's produced an increased neutron flux in the atmosphere causing a spike in radioisotopes (Clark, 2015). This caused a two-fold increase in $F^{14}C$ signatures once the testing stopped (Hua et al., 2013; Reimer et al., 2004). The spike in $F^{14}C$ declines through time due to dilution through naturally

occurring carbon cycling making it possible to accurately date post bomb testing samples based on their $F^{14}C$ signatures (Figure 3-1).

Troposphere ^{14}C levels were monitored using ^{14}C tree ring data from 1950-2009 to show the global atmospheric ^{14}C response to the bomb pulse (Hua et al., 2013). Localized post bomb ^{14}C signatures were collected from maple leaves in the Ottawa region between 1961 and 1993 and are similar to other post-bomb radiocarbon studies (McNeely, 1994). Gatineau park maple leaves from 2004-2018 were analyzed for ^{14}C by Crann (unpublished) and show $F^{14}C$ signatures of 1.08-1.01. Current $F^{14}C$ signatures resemble pre-bomb atmospheric levels as a result of the exponential decrease in atmospheric ^{14}C after the 1964 bomb pulse peak (Figure 3-1).

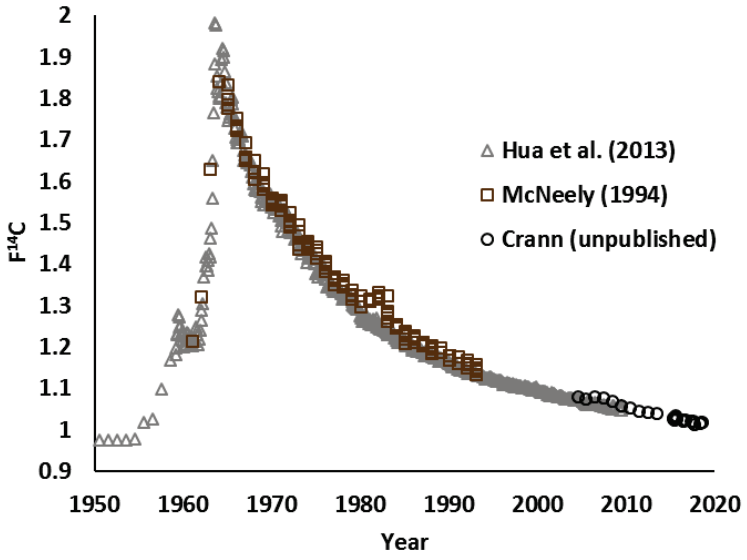

Figure 3-1. Compiled $F^{14}C$ signatures from Hua et al. (2013), McNeely (1994) and Crann (unpublished).

Many studies have shown the relationship between moisture and temperature on CO_2 production; however, the contribution of each soil horizon to the overall efflux is

specific to each system and may change depending on site specific physical and geochemical parameters. Controlled tile drainage (CTD) has an influence on such parameters as it affects field water saturation levels. Since it has been proven that moisture content can influence CO_2 production (Hashimoto & Komatsu, 2006; Moncrieff & Fang, 1999; Schaufler et al., 2010), it is expected that CTD will amplify or reduce CO_2 effluxes based on water table levels. Nangia et al. (2013) found higher CO_2 emissions in CTD fields where moisture content was elevated compared to uncontrolled tile drained (UCTD) fields. However, during drier agronomic seasons CTD and UCTD fields can exhibit similar water saturation levels which reduce variability in CO_2 emissions between the two types of fields (Van Zandvoort, Lapen, et al., 2017).

3.1.1 Purpose

The objective of this study is to better understand the production and transport of CO_2 within various soil horizons and the impact this has on CO_2 emissions. The study will use $^{14}CO_2$ signatures in conjunction with flux measurements and production rates within a soil profile at a well-studied CTD system in South-Eastern Ontario. The study is part of a larger initiative, the Agricultural Greenhouse Gases Program (AGGP) led by Agriculture and Agri-Food Canada (AAFC) to understand the influence of agricultural best management practices (BMPs) on greenhouse gas emissions.

3.2 Site Description

This study was conducted on an experimental watershed near St. Albert, Ontario on a CTD agriculture field (Site 1; Chapter 2). Samples were collected from a sampling transect at one agriculture site within the watershed. The transect included three sampling locations; field, shoulder and bank (Figure 3-2). Each location was outfitted with a surface gas and Li-COR Chambers, subsurface gas sampling rods and an area for suites of subsurface soil core sampling. The field was a soya farm field and underwent regular CTD agriculture practices. The shoulder and bank fall within the riparian zone which is classified as a grassy microecosystem with no trees.

The subsurface is characterized by a Bainsville soil series that is defined by three horizons; a surface Ap/A unit, a middle Bg layer and a basement Cg horizon (Schut & Wilson, 1987; Wicklund & Richards, 1962; Figure 3-2; Chapter 2). The Ap/A horizon is 15-30 cm and is characterized as a silty clay/loam with high organic matter content. The Ap horizon is impacted by agriculture activity and is the surface horizon in the field where the A horizon is the surface layer in the shoulder and bank. The Bg layer ranges between 25-70 cm thick and is sub divided into two unites; Bg1 and Bg2. They are mainly sandy clay loams, but the upper Bg1 unit (top 20-40 cm of the Bg horizon) contains high levels of organic matter. The B horizon is thickest in the shoulder and pinches out in the bank. The basement Cg horizon has an undefined thickness and is classified as a clay loam/heavy clay with poor drainage and low organic matter content (Chapter 2).

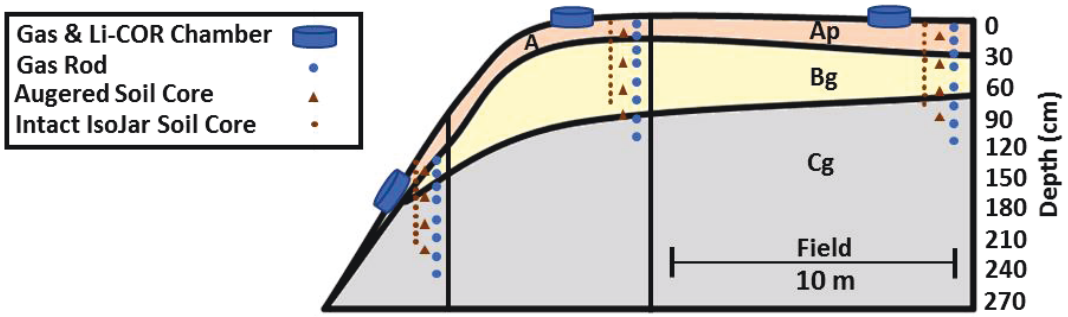

Figure 3-2. The spatial relationship between subsurface soil horizons and sampling equipment throughout the transect.

3.3 Methods

Gas chambers were used to collect gas samples for $^{14}CO_2$ analysis from the soil/atmosphere interface at each sampling location (Figure 3-2; Guitard, 2019). PVC pipe, 36 cm diameter by 20 cm high (EMCO Waterworks) were installed approximately 10 cm into the subsurface (Chapter 2). PVC pipe lid, 36 cm diameter by 5 cm high (EMCO Waterworks) was placed on each chamber for 24 hours allowing sufficient concentrations of CO_2 gas to accumulate in the chamber headspace to provide the required 1 mg of carbon for $^{14}CO_2$ analysis. A syringe was used to extract gas through a rubber septum access port and fill a 200 mL Wheaton bottle.

Intact soil cores (3" diameter) were collected between the surface and 75 cm deep at 7.5 cm intervals at all sample locations (Chapter 2; Guitard, 2019). One set of cores were collected at each location between July and August 2018. Each soil core was stored in an IsoJar container where CO_2 headspace accumulation was monitored over a four-month period. Periodic headspace samples were collected and analyzed at the University of Ottawa Ján Veizer Stable Isotope Laboratory on a SRI 8610C gas chromatograph. The observed changes in headspace concentrations over the headspace accumulation period and the mass of the sediment were used to determine CO_2 production rates at each core interval (Chapter 2).

Gas samples from the surface chambers and the IsoJars were also analyzed for $^{14}CO_2$ (Guitard, 2019). Stainless steel vacuum lines and graphitization ovens were used to solidify the CO_2 gas samples as elemental carbon and prepare them for AMS analysis (St-

Jean et al., 2017). The graphitized samples were analyzed for ^{14}C at the A.E. Lalonde AMS Laboratory at the University of Ottawa. Results were reported as $D^{14}C$ and $F^{14}C$. Modern ^{14}C dates were determined by comparing the sample's $F^{14}C$ signatures to those of known values (Hua et al., 2013; McNeely, 1994; Crann, unpublished; Figure 3-1).

Soil surface CO_2 flux chambers (19 cm diameter by 15 cm; EMCO Waterworks) were inserted 10 cm into the soil surface at the three sampling locations (Figure 3-2). A Li-COR LI-8100A CO_2 flux analyzer outfitted with a 20 cm diameter survey chamber was used to measure real-time CO_2 fluxes over a two-minute interval from the flux chamber. Li-COR measurements were collected on a weekly basis throughout the 2018 agronomic season.

Subsurface CO_2 samples were collected using ¼" gas sampling rods in the field, shoulder and bank at depths of 10 cm, 20 cm, 30 cm, 40 cm, 60 cm, 80 cm, 100 cm and 120 cm at the same sampling frequency as the surface gas samples. Samples were analyzed on an SRI 8610C gas chromatograph at Carleton University. Gas sampling and analysis methods follow the same procedures specified in Chapter 2.

Subsurface gas fluxes were calculated using measured moisture content, concentration gradients and porosity values from Bainsville retention curves (Chapter 2). Fick's law was used to calculate a flux between each subsurface sampling interval (Mayer et al., 2002; Chapter 2). A mean flux from each interval was calculated for the entire 2018 agronomic season and used to create an average flux profile for each

sampling location. The subsurface fluxes were plotted with mean surface flux values (averaged over the entire 2018 agronomic season) to show a complete flux profile. Only surface flux values with corresponding subsurface data were used to calculate a mean surface flux. Subsurface CO_2 concentrations from each sample location and depth were averaged to provide a mean concentration profile and show the relationship between mean concentrations and fluxes over the 2018 agronomic season.

A suite of augered soil cores (2.5" diameter) were collected in the field, shoulder and bank at four depth intervals; 0-15 cm, 15-40 cm, 40-65 cm and 65-90 cm on August 7th, 2018 (Chapter 2). The samples were analyzed for total carbon (TC) and total inorganic carbon (TIC) on a LECO CR-12 Carbon System (781-600) at AAFC. The difference in TC and TIC content was used to determine total organic carbon (TOC) content.

Subsurface moisture levels were recorded weekly throughout the 2018 agronomic season using a Moisture Point time domain reflectometry system. A single profiling probe was installed at 20 cm in the bank and at 15 cm, 30 cm, 45 cm, 60 cm and 90 cm in the shoulder and field. Water saturation levels were determined by moisture content in-field measurements and porosity values from Bainsville series retention curves. Qualitative observations coupled with the measured 20 cm moisture levels were used to estimate the deeper moisture content at the bank (Chapter 2; $\geq$ 40 cm depth). Water saturation levels throughout the 2018 agronomic season were averaged to create a mean water saturation profile at each sampling location.

3.4 Results

3.4.1 IsoJar Experiment

CO_2 production from IsoJar experiments show a decreasing trend with sample depth (Figure 3-3). The samples collected from the field sampling location have a maximum production rate of 64.9 μmol kg^{-1} day^{-1} which occurs at 7.5 cm depth. Production rates decrease from 7.5 cm to 37.5 cm and reach a minimum rate of 17.5 μmol kg^{-1} day^{-1}. Production slightly increases throughout the remainder of the profile reaching a rate of 28.9 μmol kg^{-1} day^{-1} at 75.0 cm. The maximum production rate in the shoulder samples is 85.8 μmol kg^{-1} day^{-1} at 15.0 cm and is the highest production rate among the three profiles. Production rates generally decrease with depth and reach a minimum value of 28.8 μmol kg^{-1} day^{-1} at 67.5 cm. In the bank, the upper 30.0 cm profile shows production rates ranging from 45.1-75.6 μmol kg^{-1} day^{-1} with a maximum at 7.5 cm. There is a sharp decrease from the 61.6 μmol kg^{-1} day^{-1} at 30.0 cm to 7.9 μmol kg^{-1} day^{-1} at 52.5 cm. Production rates remain low between 52.5-75.0 cm ranging between 7.9-2.1 μmol kg^{-1} day^{-1}.

Shallow $^{14}CO_2$ results are similar between the three profiles showing a $D^{14}CO_2$ increase from surface values between 16.0‰ and 23.8‰ and the 22.5 cm deep values between 44.1‰ and 57.9‰. Samples from below 22.5 cm show a decrease in $D^{14}CO_2$ values; however, their range varies between each sampling locations. $D^{14}CO_2$ values decrease to 4.4‰ in the field profile, 29.2‰ in the shoulder profile, and 0.1‰ in the bank profile (lowest $D^{14}CO_2$ observed; Figure 3-3).

3.4.2 Soil Carbon Content

All sampling locations show similar carbon content trends with TIC values remaining relatively constant and TOC decreasing with depth (Figure 3-3). TIC values range between 0.20-0.65% throughout all three profiles. Field TOC values range from 1.67-2.21% in the upper 40 cm and decreases to 0.12% at 65 cm and 90 cm. In the shoulder profile, TOC values in the top 40 cm range between 1.97-2.03% with a steady decrease to 0.24% at 90 cm. The maximum TOC value in the bank profile is 1.46% at 15 cm which decreases to 0.45 at 40 cm and remains low between 40-90 cm with values of 0.28-0.50%.

3.4.3 CO_2 Fluxes and Subsurface Concentrations

CO_2 concentrations are at atmospheric levels at the surface (0 cm) and increase with depth (Figure 3-3). The shoulder and bank have similar profiles with maximum values at approximately 10000 ppm at depths of 120 cm and 80 cm, respectively. Higher concentrations are observed in the field than the other sampling locations with a maximum value approaching 25000 ppm at 60 cm depth.

Highest fluxes occur at the surface and decrease with depth at each sampling location (Figure 3-3). Positive fluxes represent an upward flux and negative fluxes represent a downward flux. Mean surface flux measurements are 1.1×10^2 kg ha^{-1} day^{-1}, 2.0×10^2 kg ha^{-1} day^{-1}, and 1.4×10^2 kg ha^{-1} day^{-1}, for the field, shoulder and bank profiles, respectively. For the field and shoulder profiles, fluxes decrease gradually to 40 cm depth and range from $< 1.0 \times 10^{-1}$ kg ha^{-1} day^{-1} to 1.7×10^1 kg ha^{-1} day^{-1} from 40 cm

and below. There is a sharper decrease in the bank profile between the surface and 10 cm. Below 10 cm, there is a slight flux decrease from 1.4×10^{1} kg ha^{-1} day^{-1} to $< 1.0 \times 10^{-1}$ kg ha^{-1} day^{-1}.

3.4.4 Moisture

Moisture content is highest in the bank with mean shallow (10-30 cm depth) water saturation levels ranging from 58.7% to 61.0% and deeper (≥ 40 cm depth; Figure 3-3) water saturation levels of approximately 90.0%. Moisture content at ≥ 40 cm depth in the bank was determined to be close to water saturation based on qualitative observations from moisture rich core samples; however, these depths yielded gas samples which is why they were considered to be 90.0% saturated. The shoulder has a mean water saturation level of 30.0% at 10 cm which increases to a mean maximum water saturation level of 77.7% at 60 cm. Water saturation decreases to 54.5% at greater depths. The field shows the same trend but has higher water saturation levels throughout the profile. Mean water saturation levels increase from 42.7% at 10 cm to a mean maximum of 93.3% at 40 cm. Water saturation decreases to 70.4-76.2% below 40 cm.

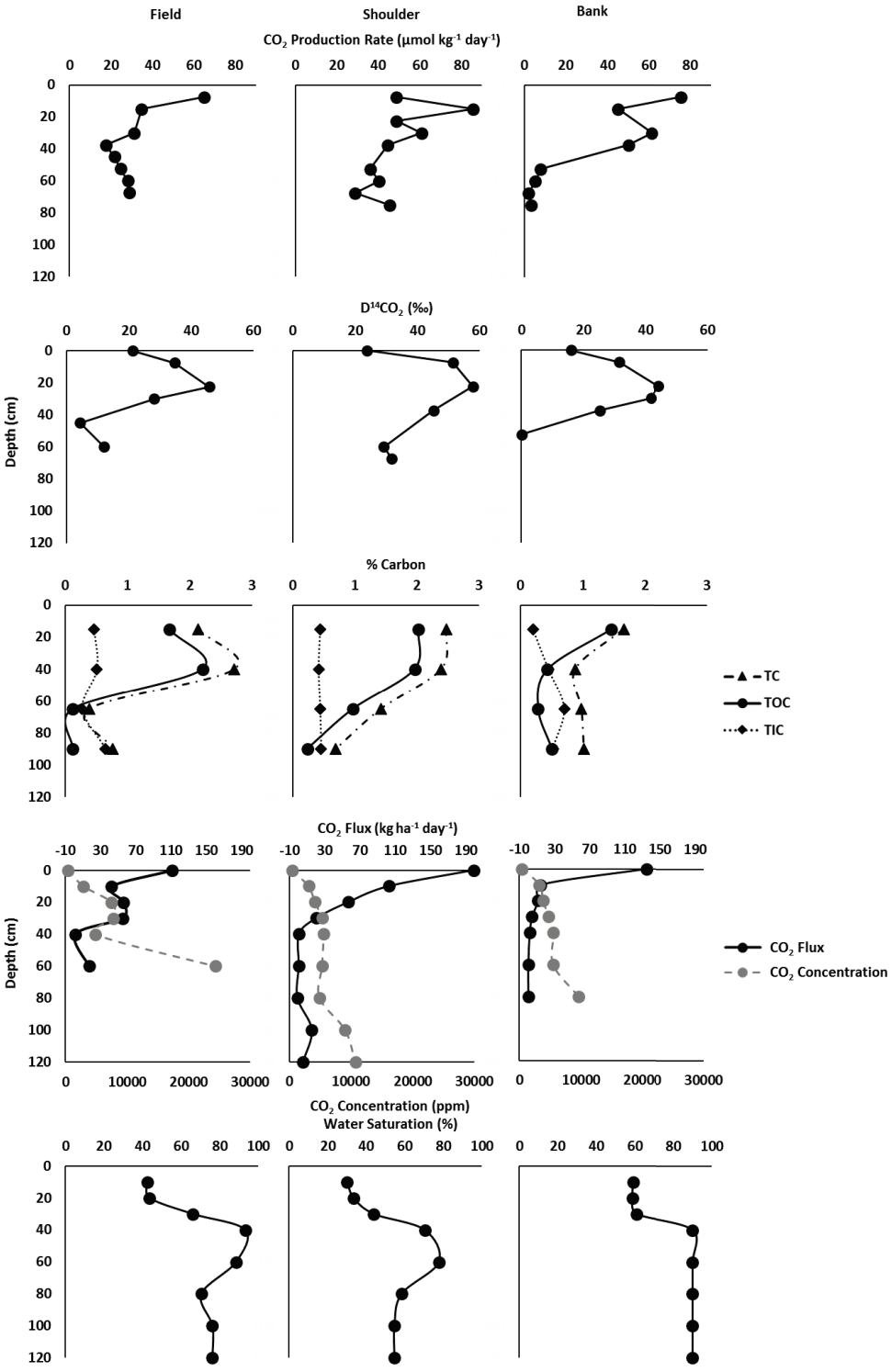

Figure 3-3. CO_2 and $^{14}CO_2$ data from the IsoJar experiments, carbon content from soil cores, CO_2 fluxes, CO_2 concentrations and moisture content are shown at the field, shoulder and bank sampling locations. CO_2 production rates are reported as µmol kg^{-1} day^{-1} and $^{14}CO_2$ values are reported as $D^{14}C$ (‰). Soil core TC, TOC and TIC are reported as % carbon. Mean subsurface CO_2 fluxes are plotted with mean surface CO_2 fluxes. They are reported as kg ha^{-1} day^{-1} and plotted with subsurface CO_2 concentrations which are reported as ppm. Mean moisture content is reported as water saturation (%). All results are reported at the lowest depth of the sampling interval.

3.5 Discussion

3.5.1 CO_2 Production and Transport

This study site contains well aeriated surface soil horizons with elevated TOC content in the A and upper Bg horizons. These oxygen rich surface layers are linked to high CO_2 production as they provide ideal conditions for root and soil respiration to proceed (Eq 3.1). Soil regions with higher oxygen availability are linked to greater CO_2 production and gas exchange with the atmosphere (B. C. Ball, 2013). The high production zones from the IsoJar experiments relate to the elevated TOC content observed in the upper soil core samples indicating a relationship between organic matter content and CO_2 production. The bank has low TOC content at 40 cm but the 37.5 cm IsoJar core still shows high production rates. Variations in organic compounds will exhibit different decomposition rates (Moncrieff & Fang, 1999). If the low TOC content is related to labile carbon compounds, it can still facilitate high production rates. Also, the banks lower Bg horizon has a mean water saturation of 61% which falls within the ideal water saturation range to enhance respiration rates (Schaufler et al., 2010). Even though the lower Bg horizon has lower TOC than the surface horizon, there is enough organic content to allow sufficient CO_2 production to occur due to the physical characteristics of the subsurface and the types of organic matter present.

The deeper field and shoulder profiles ($\geq$ 40 cm depth) have lower TOC levels than the upper layer. TOC content decreases by 95% at those deeper depths although production decreases by 41%. Moisture is still within the ideal water saturation window which enhances production rates even if there is less organic material available. The

deeper bank cores (65 and 90 cm depth) show low production even though they have similar TOC content as the higher CO_2 producing 40 cm core. The deeper cores contain moisture levels of ≥ 90% water saturation which are known to drastically reduce CO_2 production based on the scarce supply of oxygen (Moncrieff & Fang, 1999). Organic matter is crucial in facilitating root and soil respiration; however, physical parameters can enhance or limit net production as they control the conditions for these production reactions to occur.

The CO_2 flux profiles exhibit the same trends as the IsoJar production rates as high fluxes are observed in the high production zone and low fluxes in the low production zone. However, these high production regions show variable production rates throughout the upper 30-37.5 cm soil where fluxes follow an increasing trend. This relationship illustrates that high production is related to increased transport but is not the limiting control on CO_2 migration in these soil horizons since diffusion coefficients (D_i) remain constant (0.160 $cm^2\ s^{-1}$). Physical flow paths are defined by the soil's tortuosity (T_g) which is influenced by moisture content and porosity (φ; Mayer et al., 2002; Millington, 1959; Chapter 2);

$$J_i = -D_i S_g T_g \varphi \frac{\partial c}{\partial z} \quad (3.4)$$

$$T_g = {S_g}^{7/3} \varphi^{1/3} \quad (3.5)$$

Gas phase saturation (S_g) decreases with moisture content and increases the length of migration pathways which are mathematically defined by a lower tortuosity term. Longer transport pathways increase the time it takes CO_2 to diffuse vertically through the system which decreases the flux (J_i). This is demonstrated in the flux profile at the bank where low fluxes are observed in a high production zone between 7.5 cm and 30.0 cm.

High production occurs where the augered cores are observed to exhibit higher degrees of water saturation (≥ 59%) even though they display high concentration gradients ($\partial c/\partial z$; Figure 3-3). The shoulder has similar production rates throughout the upper 37.5 cm of the subsurface but shows an increasing flux with decreasing depth through that soil body. The reduced water saturation levels (30.0-43.9%) in the upper shoulder subsurface increases the connectivity between the vertical pore network which amplifies the CO_2 flux even though production rates are similar to the top 37.5 cm in the bank.

At all sampling locations, fluxes and production rates remain consistently low at and below 40 cm, although concentrations of CO_2 are high. Deeper horizons will exhibit lower fluxes due to elevated moisture content, but these lower fluxes result in higher concentrations despite the lower production rates (Figure 3-3; Chapter 2).

3.5.2 Radiocarbon Dating and CO_2 Transport

IsoJar radiocarbon signatures are related to known $F^{14}C$ signatures to determine the age of the sequestered carbon that is producing CO_2. Subsurface soil characteristics and tillage depth is used to relate an age to the $F^{14}C$ signatures. Low $F^{14}C$ signatures (approaching 1) can represent recent sequestered carbon or 1950's sequestered carbon (Figure 3-1). It is reasonable to interpret deeper cores to be older than surface samples; therefore, samples at 22.5 cm and above are interpreted to represent samples on the decreasing limb of the bomb pulse (carbon age > 1964) and samples below 22.5 cm are interpreted to be from the rising limb of the bomb pulse and dated as ≤ 1964 carbon (Figure 3-1; Table 3-1).

The samples from all sampling location show two distinct carbon ages; ≥ 2009 and ≤ 1964 with a trend of increasing age with depth (Table 3-1). The bank produces a younger surface $F^{14}CO_2$ signature (2018) than the field (2016) and shoulder (2015). However, despite the field and shoulder exhibiting similar shallow soil properties, the field has a slightly younger carbon profile than the shoulder at ≤ 22.5 cm depth. The shallow samples at the field are from the Ap horizon which is subjected to tillage that re-works the soil annually. This homogenizes the tillage layer re-distributing organic content within the surface horizon (Alvarez et al., 1995) which may cause the $^{14}CO_2$ signature at the field to reflect younger carbon.

Location	Depth (cm)	$D^{14}CO_2$ (‰)	+/- (‰)	$F^{14}CO_2$	+/- (‰)	Age
Field	0	21.2	1.8	1.0212	0.0018	2016
	7.5	34.7	1.9	1.0347	0.0019	2015
	22.5	45.9	2.0	1.0459	0.0020	2011
	30	28.1	2.0	1.0281	0.0020	≤1964
	45	4.4	1.8	1.0044	0.0018	≤1964
	60	12.0	1.8	1.0120	0.0018	≤1964
Shoulder	0	23.8	2.2	1.0238	0.0022	2015
	7.5	51.4	1.8	1.0514	0.0018	2010
	22.5	57.9	1.8	1.0579	0.0018	2009
	37.5	45.3	1.9	1.0453	0.0019	≤1964
	60	29.2	1.7	1.0292	0.0017	≤1964
	67.5	31.9	1.9	1.0319	0.0019	≤1964
Bank	0	15.9	1.9	1.0159	0.0019	2018
	7.5	31.5	2.0	1.0315	0.0020	2015
	22.5	44.1	1.9	1.0441	0.0019	2011
	30	41.7	1.8	1.0417	0.0018	≤1964
	37.5	25.2	2.0	1.0252	0.0020	≤1964
	52.5	0.1	2.0	1.0001	0.0020	≤1964

Table 3-1. $^{14}CO_2$ ages from $F^{14}CO_2$ signatures. Ages are determined by comparing sample $F^{14}CO_2$ signatures to atmospheric bomb pulse values and ages (Figure 3-1).

The $^{14}CO_2$ signature measured from the surface flux chamber will display a mixed $^{14}CO_2$ signature comprised of components from all contributing soil horizons. The surface flux chamber $^{14}CO_2$ age is 2018 (year it was collected) at the bank which suggests that the upper A horizon is producing CO_2 from newly sequestered carbon which is the dominant source for the CO_2 emitted at the surface. The shallow subsurface CO_2 samples (7.5-22.5 cm) with relatively recent sequestered carbon (2011-2015), are not reflected in the surface chamber sample. This indicates that carbon from these depths have a negligible contribution to the CO_2 efflux on the bank. This is consistent with the flux measurements, which show a 10x greater surface flux than the shallow subsurface fluxes. The bank has a shallow CO_2 emitting horizon that is generally disconnected from the rest of the soil profile as shown by the IsoJar and surface chamber $^{14}CO_2$ data.

The field and shoulder are emitting $^{14}CO_2$ with a 2016 and 2015 signature which indicates that older sequestered subsurface carbon must be influencing net CO_2 emissions. Samples from the Ap and A horizon contain 2009-2016 carbon, indicating that CO_2 from this older carbon is mixing with CO_2 from more recent carbon near the soil/atmosphere interface producing the 2015-2016 $^{14}CO_2$ signature in the surface flux chambers. The flux profile shows higher fluxes in the Ap and A horizons than the deeper soil bodies demonstrating that as depth decreases the contribution to the overall efflux increases.

Each depth profile displays $\leq$ 1964 $^{14}CO_2$ in the deeper samples indicating that there is a disconnect between carbon cycling in the upper and lower regions of this

system. The regions with older $^{14}CO_2$ are where low flux horizons are observed. The lack of ≤1964 $^{14}CO_2$ traces in shallow samples supports the interpretation that CO_2 from the lower Bg and Cg horizon undergoes minimal vertical transport and has negligible influence on surface CO_2 effluxes.

3.6 Conclusion

Within each of the three sampling profiles, in-field, shoulder and bank, highest fluxes occur at the soil/atmosphere interface where a large flux gradient is observed at the surface. The gradient is shallower between 10-30 cm depth and remains consistently low below 40 cm. Variation in production rates contribute to CO_2 transport which is reflected in the concentration profiles. CO_2 fluxes are also driven by physical parameters such as moisture which can influence migration pathways by altering the soil's gas-filled porosity and tortuosity as well as enhancing or limiting CO_2 production based on water saturation levels. Elevated production rates are associated with high organic matter content and water saturation levels of 40%. These conditions are prevalent in the shallow soil horizons where higher production and fluxes are observed and as a result have lower CO_2 concentrations.

$F^{14}CO_2$ signatures indicate that recently sequestered carbon found in the A/Ap horizons is contributing to surface CO_2 emissions. The deeper soil horizons contain older carbon that doesn't have a significant influence on the CO_2 detected in the surface chambers.

Signatures of $^{14}CO_2$ help elucidate the subsurface flux model and show that $^{14}CO_2$ is a useful indicator to study CO_2 mobility within terrestrial carbon pools. CO_2 is an important component of the carbon cycle and has a major influence on the carbon budget within agriculture systems. Understanding the fate of CO_2 transport is important to

developing mitigation strategies and can enhance our ability to reduce GHG emissions from agriculture systems.

3.7 References

Alvarez, R., Díaz, R. A., Barbero, N., Santanatoglia, O. J., & Blotta, L. (1995). Soil organic carbon, microbial biomass and CO_2-C production from three tillage systems. *Soil and Tillage Research*, *33*(1), 17–28. https://doi.org/10.1016/0167-1987(94)00432-E

Ball, B. C. (2013). Soil structure and greenhouse gas emissions: A synthesis of 20 years of experimentation. *European Journal of Soil Science*, *64*(3), 357–373. https://doi.org/10.1111/ejss.12013

Bolin, B., Degens, E., & Ketner, P. E. (1979). *The Global Carbon Cycle*. New York: Wiley and Sons.

Clark, I. (2015). *Groundwater geochemistry and isotopes*. *Groundwater Geochemistry and Isotopes*. https://doi.org/10.1201/b18347

Cole, C., Duxbury, J., & Freney, J. (1997). Global estimates of potential mitigation of greenhouse gas emissions by agriculture. *Nutrient Cycling in Agroecosystems*, *49*(1–3), 221–228. https://doi.org/10.1023/A:1009731711346

Crann, C. A., Murseli, S., Xiaolei, G. S., Ian, Z., & Kieser, W. E. (2017). First Status Report on Radiocarbon Sample Preperation Techniques at the A.E. Lalonde AMS Laboratory (Ottawa, Canada). *Radiocarbon*, *59*(3), 695–704. https://doi.org/10.1017/RDC.2016.55

ECCC. (2018). *National Inventory Report 1990–2016: Greenhouse Gas Sources and Sinks in Canada*. Retrieved from https://www.canada.ca/en/environment-climate-

Fierer, N., Allen, A. S., Schimel, J. P., & Holden, P. A. (2003). Controls on microbial CO_2 production: A comparison of surface and subsurface soil horizons. *Global Change Biology*, *9*(9), 1322–1332. https://doi.org/10.1046/j.1365-2486.2003.00663.x

Gregorich, E. G., Greer, K. J., Anderson, D. W., & Liang, B. C. (1998). Carbon distribution and losses: Erosion and deposition effects. *Soil and Tillage Research*, *47*(3–4), 291–302. https://doi.org/10.1016/S0167-1987(98)00117-2

Gregorich, E. G., Rochette, P., VandenBygaart, A. J., & Angers, D. A. (2005). Greenhouse gas contributions of agricultural soils and potential mitigation practices in Eastern Canada. *Soil and Tillage Research*, *83*(1 SPEC. ISS.), 53–72. https://doi.org/10.1016/j.still.2005.02.009

Guitard, E. (2019). *Tracing CO_2 Emissions from Agricultural Soil Respiration with Bomb Pulse ^{14}C*. University of Ottawa.

Gunter, W. D., Wong, S., Cheel, D. B., & Sjostrom, G. (1998). Large CO_2 sinks: Their role in the mitigation of greenhouse gases from an international, national (Canadian) and provincial (Alberta) perspective. *Applied Energy*. https://doi.org/10.1016/S0306-2619(98)00042-7

Hashimoto, S., & Komatsu, H. (2006). Relationships between soil CO_2 concentration and CO_2 production, temperature, water content, and gas diffusivity: Implications for field studies through sensitivity analyses. *Journal of Forest Research*, *11*(1), 41–50. https://doi.org/10.1007/s10310-005-0185-4

Hua, Q., Barbetti, M., & Rakowski, A. Z. (2013). Atmospheric Radiocarbon for the Period 1950–2010. *Radiocarbon*, *55*(4), 2059–2072. https://doi.org/10.2458/azu_js_rc.v55i2.16177

Janzen, H. H. (2004). Carbon cycling in earth systems - A soil science perspective. *Agriculture, Ecosystems and Environment*, *104*(3), 399–417. https://doi.org/10.1016/j.agee.2004.01.040

Kovaltsov, G. A., Mishev, A., & Usoskin, I. G. (2012). A new model of cosmogenic production of radiocarbon 14 C in the atmosphere. *Earth and Planetary Science Letters*, *337–338*, 114–120. https://doi.org/10.1016/j.epsl.2012.05.036

Lal, R. (2004). Soil carbon sequestration to mitigate climate change. *Geoderma*, *123*(1–2), 1–22. https://doi.org/10.1016/j.geoderma.2004.01.032

Maier, M., & Schack-Kirchner, H. (2014). Using the gradient method to determine soil gas flux: A review. *Agricultural and Forest Meteorology*, *192–193*, 78–95. https://doi.org/10.1016/j.agrformet.2014.03.006

Mayer, K. U., Frind, E. O., & Blowes, D. W. (2002). Multicomponent reactive transport modeling in variably saturated porous media using a generalized formulation for kinetically controlled reactions. *Water Resources Research*, *38*(9), 13-1-13–21. https://doi.org/10.1029/2001wr000862

McNeely, R. (1994). Long Term Enironmental Monitoring of ^{14}C Levels in the Ottawa Region. *Environment International*, *20*(5), 675–679.

Millington, R. J. (1959). Gas Diffusion in Porous Media. *Science*, *130*, 100–102.

Moncrieff, J. B., & Fang, C. (1999). A model for soil CO_2 production and transport 1: Model development. *Agricultural and Forest Meteorology*, *95*(4), 225–236.

Nangia, V., Sunohara, M. D., Topp, E., Gregorich, E. G., Drury, C. F., Gottschall, N., & Lapen, D. R. (2013). Measuring and modeling the effects of drainage water management on soil greenhouse gas fluxes from corn and soybean fields. *Journal of Environmental Management*, *129*, 652–664. https://doi.org/10.1016/j.jenvman.2013.05.040

Oertel, C., Matschullat, J., Zurba, K., Zimmermann, F., & Erasmi, S. (2016). Greenhouse gas emissions from soils—A review. *Chemie Der Erde - Geochemistry*, *76*(3), 327–352. https://doi.org/10.1016/j.chemer.2016.04.002

Reimer, P. J., Brown, T. A., & Reimer, R. W. (2004). Reporting and calibration of post-bomb ^{14}C data. *Radiocarbon*.

Schaufler, G., Kitzler, B., Schindlbacher, A., Skiba, U., Sutton, M. A., & Zechmeister-Boltenstern, S. (2010). Greenhouse gas emissions from European soils under different land use: Effects of soil moisture and temperature. *European Journal of Soil Science*, *61*(5), 683–696. https://doi.org/10.1111/j.1365-2389.2010.01277.x

Schut, L. W., & Wilson, E. A. (1987). *The soils of the regional municipality of Ottawa-Carleton*. *Ontario Institute of Pedology* (Vol. 2).

Sheridan, B. (1990). *Radiocarbon Dating*. University of Califronia.

St-Jean, G., Kieser, W. E., Crann, C. A., & Murseli, S. (2017). Semi-Automated Equipment for CO_2 Purification and Graphitization at the A.E. Lalonde AMS Laboratory (Ottawa, Canada). *Radiocarbon*, *59*(3), 941–956. https://doi.org/10.1017/RDC.2016.57

Stenström, K. E., Skog, G., Georgiadou, E., Genberg, J., & Johansson, A. (2011). *A guide to radiocarbon units and calculations*. Lund.

Stuiver, M., & Polach, H. A. (1977). Discussion Reporting of ^{14}C Data. *Radiocarbon*, *19*(3), 355–363.

Stumm, W., & Morgan, J. J. (2012). *Aquatic Chemistry: chemical equilibria and rates in*

natural waters (3rd ed.). New York: John Wiley & Sons.
Wicklund, R. E., & Richards, N. R. (1962). Soil Survey of Russell and Prescott Counties. *Ontario Soil Survey*, (33).
Van Zandvoort, A., Lapen, D. R., Clark, I. D., Flemming, C., Craiovan, E., Sunohara, M. D., et al. (2017). Soil CO_2, CH_4, and N_2O fluxes over and between tile drains on corn, soybean, and forage fields under tile drainage management. *Nutrient Cycling in Agroecosystems*, *109*(2), 115–132. https://doi.org/10.1007/s10705-017-9868-4

4.0 Conclusion and Future Recommendations

This study showed that there is minimal spatial variation in GHG surface emissions as vegetation cover changed. At each site, the field, shoulder and bank showed comparable GHG surface fluxes except for methane (efflux at the site 10 bank and influx at all other sampling locations) despite the field containing agricultural crops and the riparian zones consisting of natural vegetation. The variation in methane fluxes is credited to changes in redox environment, not vegetation cover. Site 1 has a grassy riparian zone which slightly differs from the shrubs and trees that make up the riparian zone at site 10. Despite the two riparian zones exhibiting variable vegetation cover, they both display comparable GHG emissions.

Surface fluxes are mainly driven by subsurface moisture content and concentration gradients. Moisture content increases with depth which decrease GHG transport. Shallow soil horizons show higher GHG concentration gradients than the underlying bodies. The combination of higher gradients and lower moisture content enhances GHG transport in the surface soil horizons.

CO_2 surface fluxes are mainly influenced by the shallow, high flux regions of the subsurface. CO_2 concentration increases with depth where there is reduced production and low transport. High production in a low concentration zone is indicative that there is elevated transport reducing the measured CO_2 in shallow soils. Surface $^{14}CO_2$ signatures resemble those from the shallow soil horizons which support the interpretation surface emissions are directly related to shallow subsurface production and transport. Deeper

soils have an older $^{14}CO_2$ signature that is not observed at the surface.

Comparing surface GHG fluxes to subsurface GHG measurements, physical soil properties and aqueous geochemistry gives us meaningful insight on GHG transport mechanisms. However, we have yet to accurately identify microscale production and consumption rates within the subsurface. The IsoJar experiment shows expected production from soil at each depth but doesn't account for transport in the system. Subsurface $^{14}CO_2$ signatures may vary from those observed from the IsoJar experiment. I suggest collecting $^{14}CO_2$ samples directly from the gas rods to observe signatures that reflect CO_2 transport. I also recommend adding ^{15}N to the sampling regime. Collecting both soil and gas ^{15}N samples will help identify nitrifying and denitrifying zones within the subsurface.

It is important to continue monitoring surface GHG fluxes, subsurface GHG levels and soil properties to determine the changes that removing riparian zone vegetation has on such parameters. This study showed that the two riparian zones display similar soil properties and produce comparable surface fluxes. Dredging one riparian zone will alter its microecosystem, enhancing the contrast between the two riparian zones at WEBs. The lack of vegetation can influence subsurface soil conditions that drive GHG transport. It is important to continue this study to monitor such changes to determine the buffering capacity of naturally vegetated riparian zones.

Applying this data set to calibrate a reactive transport model at WEBs will be

useful to show the effect of land cover changes on GHG emissions and transport. Understanding those relationships and displaying them through a well calibrated model could help develop BMPs. Understanding the driving mechanisms behind GHG transport at WEBs will allow for the implementation of appropriate BMPs that were deemed effective through the other aspects of the AGGP project.